Acta Neuropathologica (2023) 145:335–355
https://doi.org/10.1007/s00401-023-02537-5

ORIGINAL PAPER

Persistent virus-specific and clonally expanded antibody-secreting cells respond to induced self-antigen in the CNS

Andreas Agrafiotis[1,2] · Raphael Dizerens[1] · Ilena Vincenti[3] · Ingrid Wagner[3] · Raphael Kuhn[1] · Danielle Shlesinger[1] · Marcos Manero-Carranza[1] · Tudor-Stefan Cotet[1] · Kai-Lin Hong[1] · Nicolas Page[3] · Nicolas Fonta[3] · Ghazal Shammas[3] · Alexandre Mariotte[3] · Margot Piccinno[3] · Mario Kreutzfeldt[3,9] · Benedikt Gruntz[1] · Roy Ehling[1] · Alessandro Genovese[2] · Alessandro Pedrioli[2] · Andreas Dounas[4] · Sören Franzenburg[5] · Hayrettin Tumani[10] · Tania Kümpfel[6,7,8] · Vladyslav Kavaka[6,7] · Lisa Ann Gerdes[6,7,8] · Klaus Dornmair[6,7,8] · Eduardo Beltrán[6,7,8] · Annette Oxenius[2] · Sai T. Reddy[1] · Doron Merkler[3,9] · Alexander Yermanos[1,2,3,11]

Received: 6 September 2022 / Revised: 20 December 2022 / Accepted: 2 January 2023 / Published online: 25 January 2023
© The Author(s) 2023

Abstract

B cells contribute to the pathogenesis of both cellular- and humoral-mediated central nervous system (CNS) inflammatory diseases through a variety of mechanisms. In such conditions, B cells may enter the CNS parenchyma and contribute to local tissue destruction. It remains unexplored, however, how infection and autoimmunity drive transcriptional phenotypes, repertoire features, and antibody functionality. Here, we profiled B cells from the CNS of murine models of intracranial (i.c.) viral infections and autoimmunity. We identified a population of clonally expanded, antibody-secreting cells (ASCs) that had undergone class-switch recombination and extensive somatic hypermutation following i.c. infection with attenuated lymphocytic choriomeningitis virus (rLCMV). Recombinant expression and characterisation of these antibodies revealed specificity to viral antigens (LCMV glycoprotein GP), correlating with ASC persistence in the brain weeks after resolved infection. Furthermore, these virus-specific ASCs upregulated proliferation and expansion programs in response to the conditional and transient induction of the LCMV GP as a neo-self antigen by astrocytes. This class-switched, clonally expanded, and mutated population persisted and was even more pronounced when peripheral B cells were depleted prior to autoantigen induction in the CNS. In contrast, the most expanded B cell clones in mice with persistent expression of LCMV GP in the CNS did not exhibit neo-self antigen specificity, potentially a consequence of local tolerance induction. Finally, a comparable population of clonally expanded, class-switched, and proliferating ASCs was detected in the cerebrospinal fluid of relapsing multiple sclerosis (RMS) patients. Taken together, our findings support the existence of B cells that populate the CNS and are capable of responding to locally encountered autoantigens.

Keywords Viral infection · Autoimmunity · CNS tolerance · Multiple sclerosis · Antibody-secreting cells

Introduction

The access of circulating immune cells into the CNS is restricted in healthy individuals under steady-state conditions with only very low numbers of lymphocytes residing in the brain. However, in CNS inflammatory conditions, the number of immune cells entering the CNS parenchyma through the blood–brain barrier or blood–cerebrospinal fluid barrier increases dramatically [2, 26, 55, 59, 67, 77]. Upon infiltration, T and B cells can adopt a wide range of phenotypes and effector functions that can either protect against pathogenic threat or, conversely, contribute to disease [25, 34, 34]. Thereby, T cells have previously

Alexander Yermanos and Doron Merkler contributed equally to this work.

✉ Doron Merkler
Doron.Merkler@unige.ch

✉ Alexander Yermanos
ayermanos@gmail.com

Extended author information available on the last page of the article

been shown to be able to locally reside in a variety of non-lymphoid tissues, including the CNS, and to adopt a tissue-resident memory phenotype (Trm) [12, 16, 21, 36, 66]. Such Trm are poised to respond to secondary exposures [70, 73, 75] or can participate in compartmentalized inflammation in the CNS [75], In contrast, much less is known about the phenotype and function of tissue-resident B cells [4, 27] and their interference with circulating counterparts. This is particularly true in the case of the CNS, where the formation and existence of resident B cells is still under debate. Yet, B cells are involved in the pathogenesis of neuroinflammatory diseases by a variety of mechanisms including antigen presentation to T cells [51], transport of antigens to secondary lymphoid organs, secretion of pro-inflammatory or anti-inflammatory cytokines [6, 23], and pathogenic antibodies [34, 64]. Furthermore, the success of B cell-depleting therapies in patients with multiple sclerosis and other chronic autoimmune conditions with presence of neuronal auto-antibodies provides compelling evidence that B cells are crucially involved in the pathophysiology of these diseases [15, 29, 39, 41, 69]. While autoreactive antibodies to various protein targets such as MOG [10], DPPX [8], and aquaporin-4 [35] have been profiled and are even used in diagnostics of certain neurological disorders [19, 60], the cellular counterparts and origins within or outside the CNS of these antibodies remain unclear. In addition, despite recent advances in the field regarding transcriptional characteristics of disease-relevant B cells subsets found in the inflamed CNS [62], whether these cells can undergo clonal selection and be locally reactivated to CNS-restricted autoantigens remains unknown.

Recent advancements in sequencing and microfluidic techniques have enabled comprehensive profiling of B cells and their corresponding antibody repertoires [1, 32, 52, 80]. Current iterations of this technology provide both single-cell antibody repertoires (full-length, paired heavy and light chain antibody sequences) and single-cell transcriptomes [17]. This results in a quantitative profile of B cell clonal selection that can further be validated via recombinant expression of antibodies of interest. However, the relationship between gene expression and B cell receptor (BCR) repertoire of CNS B cells has not yet been linked to the functional properties of their corresponding antibodies. Here, we leveraged single-cell antibody repertoire and transcriptome sequencing in combination with transgenic murine models of infection and autoimmunity to investigate the clonal selection of virus-specific B cells. We discovered populations of antigen-specific ASCs that had undergone class-switch recombination, clonal expansion, and somatic hypermutation after viral infection in the CNS. Upon induction of localized LCMV GP as a neo-self antigen in glia cells after viral clearance, we observed that ASCs adopted a proliferative transcriptional program and produced antibodies specific to the induced neo-self antigen. In contrast, such GP-specific antibodies were absent after a corresponding transient viral infection in which LCMV GP was persistently expressed as a neo-self antigen in oligodendrocytes, pointing towards a CNS-mediated tolerance mechanism. Mirroring our experimental observations, we uncovered expanded and class-switched ASCs in the cerebrospinal fluid of patients with relapsing multiple sclerosis suggesting a disease-relevant involvement of ASC in CNS autoimmunity which may serve as a starting point for future specific therapeutic approaches.

Materials and methods

Mice

The C57Bl/6J GFAP:GP (GFAP-Cre$^{ERT2\ tg/+}$;Stop-GP$^{flox/+}$) mouse line was bred by crossing C57Bl/6 GFAP-CreERT2 mice [31] expressing the TAM-inducible Cre-recombinase under the astrocyte-specific GFAP promoter with C57Bl/6J Stop-GP mice [56]. The C57BL/6J MOG:GP (MOGi$^{Cre/+}$: Stop-GP$^{flox/+}$) mouse line was generated by crossing mice expressing the Cre-recombinase under the control of the oligodendrocyte-specific promoter (MOGiCre; [33]) with Stop-GP mice, as described previously [56]. All mice were bred and lodged under specific-pathogen-free P2 conditions in the animal facilities of the University Medical Center of Geneva. Age-matched male and female sex mice between 6 and 12 weeks of age were used for experiments. Animal experiments were authorized by the cantonal veterinary office of Geneva and performed in conformity with institutional guidelines and Swiss federal regulations under license number XGE3920D.

Virus infections

The recombinant LCMV-GP58 were generated and propagated on baby hamster kidney 21 cells BHK21 (ATCC® CCL-10) [22]. Virus stocks were titrated using MC57G cells (ATCC® CRL-2295) [37]. In the recombinant LCMV-GP58, the LCMV full-length-GP was replaced by a fusion protein of the LCMV GP signal sequence including the GP_{33-41} epitope and the vesicular stomatitis virus glycoprotein (VSVG). For transient infection of the CNS, mice were intracranially injected with 10^4 plaque-forming units (PFU) of rLCMV-GP58 diluted in 30 µl of minimum essential medium (MEM, Gibco).

Tamoxifen (TAM) administration

TAM (Sigma, T5648) was dissolved in a 9:1 mix of sunflower oil and ethanol to a concentration of 10 mg/ml by mixing the solution for 20 min at 50 °C. A dose of 100 µl of TAM solution was administered intraperitoneally twice per day for 4 consecutive days.

Antibody-mediated depletion

Circulating $CD20^+$ cells were depleted by intraperitoneal administration of 200 µg of rat-anti-mouse-CD20-depleting antibody (Biolegend, 152104) 2 days before the start of TAM administration. Depletion of circulating CD20 + B cells was confirmed by flow cytometry.

Rotarod

The rotarod test was used to monitor the ability of motor coordination and balance of mice. Mice were placed on a rotating rod (Rotarod 7650; Ugo Basile Biological Research) constantly accelerating from 10 to 80 rounds per minute for a maximum of 180 s. Endurance time was monitored, and the two best runs out of three at each time point were averaged for analysis. Animals were habituated and trained to the rotarod daily from day − 3 to day 0. Displayed values (% latency to fall) are normalized to the running values of mice at day 0.

Cell isolation and flow cytometry

For the isolation of cells in the CNS, mice were anesthetized and transcardially perfused with PBS. CNS tissues were cut and digested in DMEM with Collagenase A (1 mg/ml, Roche) and DNase I (0.1 mg/ml, Roche) at 37 °C for one hour. Cells were homogenized using a 70-µm cell strainer (BD Biosciences) before leukocytes were separated using 30 and 70% Percoll gradients and subsequently stained for 30 min in FACS buffer (PBS/2.5%FCS/10 mM EDTA/0.01% NaN3) with the following primary antibodies: CD45-PacificBlue (Biolegend, 103126), CD19-biotin (Biolegend, 115503), CD3E-APC (Biolegend, 100311). Oligonucleotide barcodes conjugated to phycoerythrin (PE) and streptavidin (TotalSeq™-C0951 PE Streptavidin, TotalSeq™-C0952 PE Streptavidin and TotalSeq™-C0953) were added to biotinylated anti-CD19 antibodies to maintain sample identity following pooling of B cells for each experimental condition. CD19 + B cells were sorted individually for each mouse using a BD LSRFortessa (BD Biosciences) and BD FACSDiva (BD Biosciences, v8.0.2) using appropriate filter sets and compensation controls. B cells arising from the same experimental condition were subsequently pooled and used as input to single-cell immune repertoire sequencing. Data were analyzed using FlowJo software (v10).

Single-cell immune repertoire sequencing of murine B cells

For single-cell sequencing, brain B cells (CD19 + CD3-CD45.1 +) were FACS-sorted from STOP:GP, aCD8-GFAP:GP and GFAP:GP mice 7 days after start of TAM, and from MOG:GP mice 47 days after i.c infection. Combined single-cell transcriptome and immune repertoire sequencing was performed using the 10 × Genomics Chromium Single Cell V(D)J Reagents Kit (CG000166 Rev A) according to established methods [52]. Single cells together with gel beads (10 × Genomics, 1,000,006) were encapsulated in gel emulsion microdroplets using 4 lanes of one Chromium Single Cell A Chip (10 × Genomics, 1,000,009) with a target loading of 13,000 cells per reaction. Subsequent cDNA amplification was performed using 14 cycles. The samples were then split for separate GEX, VDJ and feature barcode library preparation (10 × Genomics, 1,000,080). GEX and feature barcode libraries were amplified using the Chromium Single Cell 5' Library Kit (10 × Genomics, 1,000,006) and BCR libraries were amplified using the Chromium Single Cell V(D)J Enrichment Kit, Mouse B Cell (10 × Genomics, 1,000,072). The final libraries were pooled and sequenced using the Illumina NovaSeq S1 platform at a concentration of 1.8 pM with 5% PhiX.

Single-cell immune repertoire sequencing of B cells from CSF of RMS and RIS patients

For single-cell sequencing of B cells in the CSF of RMS and radiologically isolated syndrome (RIS) patients, fresh CSF samples were processed within one hour after collection. CSF samples (3–6 ml) were centrifuged at 300 *g* for 10 min. The pellet was then transferred to a 2-ml tube and further processed using the 10 × Chromium Next GEM Single Cell VDJ v1.1 Reagents Kit (CG000208 Rev B) as previously described [30]. GEX and BCR libraries were sequenced on an Illumina NovaSeq6000 S4 using read lengths of 150 bp read 1, 8 bp i7 index, 150 bp read 2. The study was approved by the local ethics committee of the Ludwig-Maximilian University Munich (project no. 163-16 and 18-419), and written informed consent was granted by all participants included in the study.

Immune repertoire analysis

Raw paired-end sequencing files of the GEX, V(D)J, and feature barcode libraries were aligned to the murine reference genome (mm10), V(D)J germlines (GRCm38) and reference feature barcode sequences using 10 × Genomics

Cell Ranger (v6.0.0). Accordingly, GEX and V(D)J libraries from human samples were aligned to the human reference genome and V(D)J germlines (GRCh38). Specifically, the count argument of Cell Ranger was used to align GEX and feature barcode libraries separately while the V(D)J was aligned using the vdj argument. The filtered feature matrix GEX and V(D)J files as well as unfiltered feature barcode files were supplied into the VDJ_GEX_matrix function of the R package Platypus (v3.1) [80], which relies on the R package Seurat (v4.0.3) [65] for gene expression analysis. For human samples, cells were filtered based on CD3E, CD4 and CD8A expression to exclude T cells from the analysis. Annotations from GEX were transferred to VDJ and vice versa by matching cellular 10 × barcodes. Cells containing more than 5% mitochondrial genes were removed from transcriptome analysis. Gene expression was log-normalized with a scaling factor of 10,000 and the mean expression and variance were additionally scaled to 0 and 1, respectively. 2000 variable features were supplied as input to principal component analysis (PCA) using the "vst" selection method. The first ten dimensions were used to assign the cells to transcriptional clusters with the Seurat functions FindNeighbors and FindClusters (Satija et al. 2015) at a cluster resolution of 0.5 using a graph-based clustering approach incorporating Louvain modularity optimization and hierarchical clustering. UMAP was calculated using the first ten dimensions. Gene expression feature plots and violin plots were created by supplying selected genes to the FeaturePlot and VlnPlot functions of Seurat. The GEX_cluster_genes function from Platypus, which relies on the FindMarkers function from Seurat, was used to calculate differentially expressed genes across clusters and conditions with logfc.threshold set to 0 using the Wilcoxon Rank Sum. Mitochondrial and ribosomal genes were removed when visualizing differentially expressed genes (DEG) using the GEX_volcano and GEX_cluster_genes_heatmap functions from Platypus or supplying the top DE genes as input to GEX_volcano and GEX_gsea functions from Platypus to perform gene ontology and gene set enrichment analyses, respectively. The C7 immunological signatures gene set from the Molecular Signatures Database (MSigDB) was used as an input for the GEX_gsea function, which relies on the R package fgsea (v1.16.0) [38]. The GEX_GOterm function of Platypus is based on the R package edgeR (v3.14) [63]. Clonotyping was performed based on those B cells containing identical CDRH3 + CDRL3 amino acid sequences using the VDJ_clonotype function of the R package Platypus. Only clones containing exactly one VH and one VL sequence were included in the BCR analysis. Heatmaps visualizing the number of public clones and the VH and VL gene usage were created using the R package pheatmap (v1.0.12). For antibodies that were selected for expression in PnP-mRuby hybridoma cells, the full-length VH and VL sequences including framework region 1 to framework region 4 were annotated using MiXCR (v3.0.1) and exported by the VDJRegion gene feature.

Histology and image analyses

Mice were perfused with PFA and CNS tissue was collected, PFA fixed overnight, paraffin embedded and cut at 2um. For immunofluorescence, endogenous mouse IgG was visualized by incubating tissue sections 1 h with an AlexaFluor 647-conjugated anti-mouse IgG (JacksonImmunoresearch, 715-605-151). Sections were washed and incubated with Dako REAL peroxidase blocking solution (Dako, K0672) to inactivate endogenous peroxidases and unspecific bindings were blocked (PBS/10% FCS). Tissue sections were incubated with rabbit anti-Ki67 antibody (Abcam, ab66155) overnight at 4 °C in Dako REAL antibody diluent (Dako, S2022). To visualize the specific signal, anti-rabbit HRP (Dako, K4003) with amplification (Opal 570, Akoya, FP1488001KT) was used as a secondary system. After wash, sections were incubated with Fab fragment-goat-anti-mouse IgG (JacksonImmunoResearch, 115-007-003) and goat serum to avoid unspecific bindings. Rat anti-CD138 antibody (rat anti-CD138, clone 281-2, Biolegend, 142502) was applied to each section and specific bounds were visualized using a Alexa Fluor488-conjugated anti-rat antibody (JacksonImmunoResearch, 712-545-153). Nuclei were visualized using DAPI (Invitrogen, D1306). For immunohistochemistry, sections were incubated with Dako REAL peroxidase blocking solution (Dako, K0672) to inactivate endogenous peroxidase and Fab fragment-goat-anti-mouse IgG (JacksonImmunoResearch, 115-007-003) to avoid nonspecific bindings. Slides were incubated with a rat anti-B220 antibody (RA3-6B2, eBioscience, 14-0452-85). Bound primary antibodies were visualized with a goat anti-rat HRP (Vector Laboratories, MP-7444-15) and bound secondary antibodies with 3,3'-diaminobenzidine as chromogen (Dako, K3468) and counterstained with Hemalum (Merck, 1.09249.0500) for brightfield microscopy. Coverslips were mounted in Fluoromount aqueous mounting medium (Sigma-Aldrich, F4680) for image acquisition. Immunostained sections were scanned using Pannoramic Digital Slide Scanner 250 FLASHII (3DHISTECH) in 200 × magnification. All quantifications were performed manually using Pannoramic Viewer software (3DHISTECH). The examiner was blinded to the experimental group. For representative images, white balance was adjusted, and contrast was enhanced using the tools "levels," "curves," "brightness," and "contrast" in Photoshop CS6 (Adobe). All modifications were acquired uniformly on the entire image.

Antibody expression and validation

Selected antibodies were produced in PnP-mRuby hybridoma cells as previously described (Parola et al., 2019) and validated using normalized supernatant ELISAs against purified LCMV clone 13 NP, LCMV clone 13 GP, DNP-OVA, insulin (Sigma, I5500), mouse genomic DNA (Sigma, 692339), MOG 1-125 (Anaspec, 55158), as previously described [52]. An anti-mouse IgG-HRP (Sigma, A2554) was employed at 1:1500 and used for detection. Purified antigens were tested at 5 µg/ml while self-made extracts were tested at 100 µg/ml coating concentration. Infected MC57G cells were centrifuged for 10 min at 1600 rpm at 4 °C and the pellet was resuspended in 5 ml of PBS. Cells were lysed using a syringe (28G needle), homogenized several times and additionally sonicated (3 times 20 s at 40 MHz) on ice. Anti-mouse beta actin IgG (Sigma, A2228), anti-OVA IgG (in house), anti-NP-IgG PANK1, anti-GP-IgG Wen3.1, anti-MOG clone 8-18C5 (Sigma, MAB5680) and anti-dsDNA IgG AE-2 (Sigma, MAB1293) were used as negative and positive controls for respective experiments and employed at 4 µg/ml.

Serum ELISA

ELISA 96-well plates (Corning Incorporated) were coated with purified LCMV NP or LCMV GP at 3 mg/ml, blocked with PBS supplemented with 2% (w/v) milk (AppliChem, A0830) and incubated with fivefold serial dilutions of 1:100 pre-diluted serum (naive serum served as control). Igk binding was detected using anti-mouse kappa light chain-HRP (Abcam, ab99617) secondary antibody. Binding was quantified using the 1-Step Ultra TMB-ELISA substrate solution (Thermo, 34028) and 1 M H2SO4 for reaction termination. Absorbance at 450 nm was recorded on an Infinite 200 PRO (Tecan). All commercial antibodies were used according to the manufacturer's recommendations.

Data visualization

The graphical abstract and experimental setup were created using Biorender. The R packages ggplot (v3.3.3), ggrepel (v0.9.1), VennDiagram (v1.1.0), Seurat (v1.1.1) and gridExtra (v2.3) were used for data visualization. Donut plots and bar graphs were created using GraphPad Prism® Software version 9. All figures were assembled using Adobe Illustrator for Mac (v26.0.1).

Statistical analysis

Unless otherwise mentioned, statistical significance ($*p \leq 0.05, **p \leq 0.01, ***p \leq 0.001, ****p \leq 0.0001$) was calculated using an unpaired, two-tailed *t* test for comparing two groups or a two-way analysis of variance (ANOVA) with post hoc Tukey's multiple comparison test when multiple time points were present. All error bars represent the standard error of the mean. All statistical analyses were performed in GraphPad Prism® Software version 9 or in R using the base statistics package.

Results

Models of inducible and chronic expression of CNS-localized neo-self antigen

To characterize virus-specific and potentially autoreactive B cells in the CNS, we utilized four different experimental conditions involving viral infection and autoimmunity in the CNS (Fig. 1a). Three conditions utilized a recently described CNS autoimmune mouse model driven by brain-resident memory T cells (bTRM) [75], which involves GFAP-Cre$^{ERT2\ tg/+}$;Stop-GP$^{flox/+}$ mice (referred to as GFAP:GP). GFAP:GP mice express a tamoxifen-inducible Cre recombinase under the glial fibrillary acidic protein (GFAP) promoter driving the expression of LCMV glycoprotein (GP). The GFAP:GP model generates LCMV-GP33-41-specific bTRM by an intracranial infection with rLCMV-GP58, a recombinant LCMV strain containing the first 58 amino acids of LCMV GP fused to the vesicular stomatitis virus (VSV) glycoprotein (termed rLCMV-GP58) (Fig. 1a). Six weeks after viral clearance, intraperitoneal (i.p.) tamoxifen (TAM) administration induces full-length LCMV-GP as a neo-self antigen in astrocytes and results in bTRM reactivation and development of locomotor deficits [75]. Littermate Stop-GP$^{flox/+}$ mice, termed STOP:GP, served as post-infection controls as they lack the GFAP-Cre$^{ERT2tg/+}$ and therefore do not express the full-length LCMV GP upon TAM administration [75] (Fig. 1a). To exclude recruitment of peripheral B cells during induced neo-self antigen expression (LCMV-GP), we included an experimental condition that received i.p. administration of a B cell CD20-depleting monoclonal antibody before administration of TAM (supplementary Fig. 1a, online resource), referred to as aCD20-GFAP:GP (Fig. 1a), which was assessed at day 0 and day 7 following TAM administration (supplementary Fig. 1b, online resource). Lastly, we leveraged recently described transgenic mice that constitutively express the full-length LCMV GP under the control of the myelin oligodendrocyte glycoprotein (MOG) promoter, termed MOG:GP, to create a condition in which viral infection induces chronic autoimmune disease [57] (Fig. 1a). 6-week-old mice of the GFAP:GP, aCD20-GFAP:GP, and STOP:GP conditions were treated with TAM (6 weeks post-infection) and sacrificed seven days after initial TAM administration, while mice of MOG:GP were sacrificed 47 days after initial infection. Mice started to lose

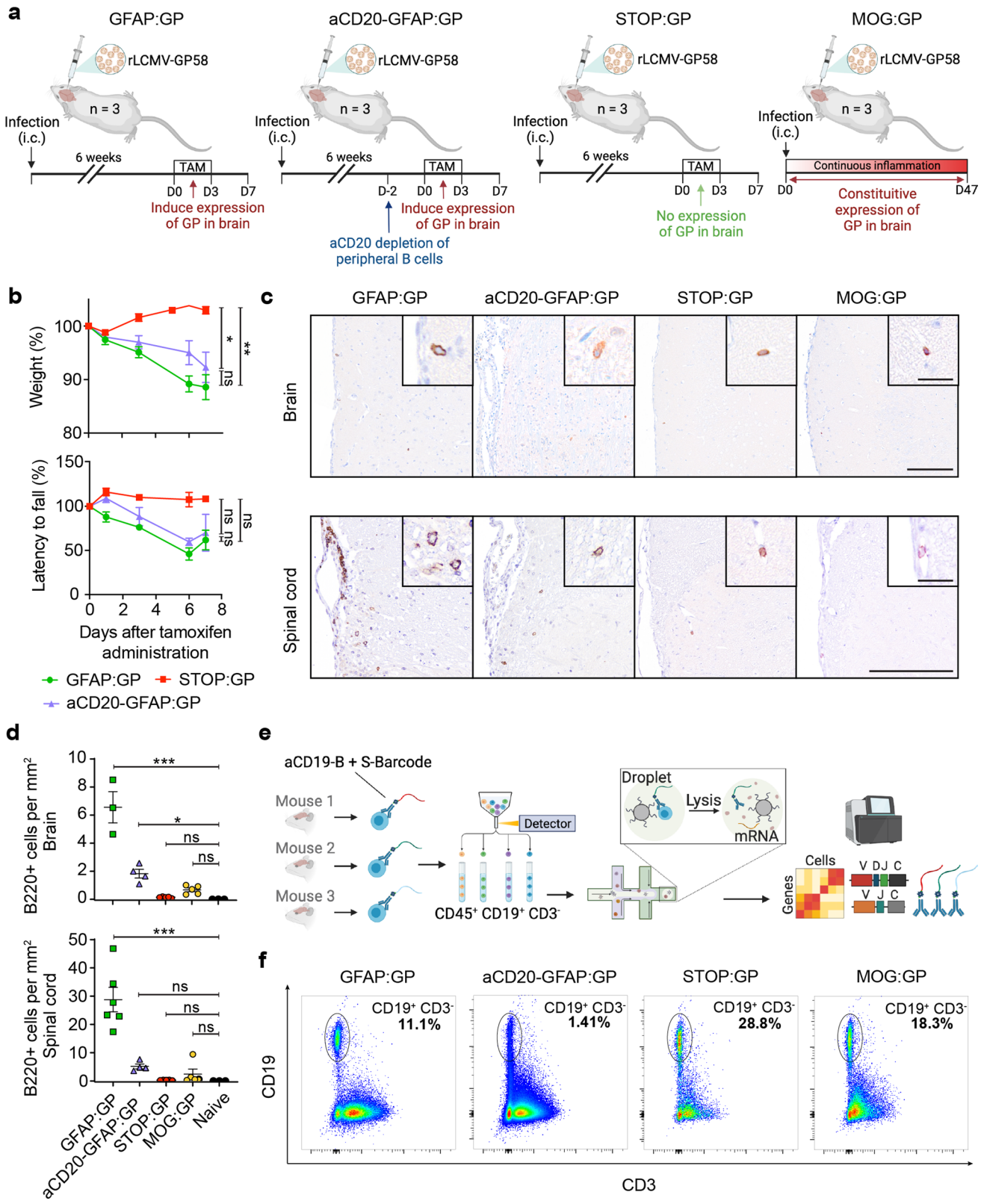

weight approximately three days following neo-self antigen induction in all groups excluding STOP:GP mice (Fig. 1b). Furthermore, all groups losing weight demonstrated locomotor impairments and ataxia based on reduced performance on the rotarod test (Fig. 1b). Together, this revealed that circulating CD20-expressing B cells are not required for

◂**Fig. 1** Models of inducible and chronic expression of CNS-localized self-antigen. **a** Experimental overview of intracranial (i.c.) infection and models of autoimmunity. **b** Weight loss (top) and rotarod performance measuring locomotor impairment and ataxia (bottom), where symbols represent one individual mouse group and bars represent means ± SEM. $*p < 0.05$; ns, not significant; two-way ANOVA followed by Tukey's multiple comparisons test (three mice per group). **c** Representative immunostainings and **d** quantification of B220 + cells in brain and spinal cord sections of indicated groups. Tissues were collected 7 days after tamoxifen treatment, except for the MOG:GP group, where tissue collection occurred 50 days post infection. Scale: 150 um. Inset: 20 um. Symbols represent one individual mouse, and bars represent means ± SEM. $*p < 0.05$, $**p < 0.01$ $***p < 0.001$; ns, not significant; one-way ANOVA followed by Dunnett's multiple comparisons test. **e** Fluorescent activated cell sorting strategy to isolate $CD19^+$ expressing cells from murine brains followed by library construction and single-cell sequencing. **f** Representative flow cytometry dot plots illustrating the gating strategy of the pre-sorted $CD19^+/CD3^-$ B cell populations per mouse for each experimental group. One representative mouse per group is shown with the percentage of the sorted population indicated

the observed disease in the previously described GFAP:GP model of autoimmunity despite histology revealing a significant increase in B220 + cell number in brains and spinal cords of GFAP:GP mice compared to naive mice (Fig. 1c, d).

Single-cell immune repertoire sequencing reveals heterogeneous populations of CNS B cells following infection and autoimmunity

Given previous findings demonstrating B cell infiltration in GFAP:GP, STOP:GP and MOG:GP conditions [57, 75], in conjunction with our observed disease manifestations (Fig. 1b), we questioned whether single-cell immune repertoire sequencing would provide insight into selection fingerprints of CNS B cells and their functional role in the context of CNS infection and autoimmunity. We therefore isolated brain-infiltrating B cells using flow cytometry and anti-CD19 antibodies tagged with mouse-specific oligonucleotide barcodes (Fig. 1e). Sorted $CD19^+/CD3^-$ B cells (Fig. 1f, supplementary Fig. 1c, online resource) from three mice per group were pooled for each of the aforementioned experimental conditions (Fig. 1a) and subjected to single-cell sequencing of their antibody repertoires, transcriptomes, and mouse-specific oligonucleotide barcodes (Fig. 1e). Following library construction, deep sequencing, and alignment to reference genomes, we recovered a total of 22,444 single cells per condition with an average of 766 genes per cell and a low percentage (~ 1–3%) of reads mapping to mitochondrial genes (supplementary Fig. 2a, b, c, online resource). The fractions of cells assigned to each mouse-specific oligonucleotide barcode were comparable within all experimental conditions for both the transcriptomes and antibody repertoires with only a minor fraction (~ 5%) of cells that could not be assigned to any of the barcodes (supplementary Fig. 2d, online resource), thereby signifying high reproducibility across mice.

We performed uniform manifold approximation projection (UMAP) and unsupervised clustering for an unbiased overview of all cell populations based on global gene expression (Fig. 2a, supplementary Fig. 3, online resource). This revealed that cells arising from STOP:GP and MOG:GP mice occupied multiple clusters at comparable frequencies, indicating that brain-infiltrating B cells after long-term CNS autoimmunity are transcriptionally similar to steady-state B cells generated via infection. Cells from GFAP:GP were present in the majority of observed clusters but were especially present in cluster 0 (Fig. 2b, c), whereas cells arising from the aCD20-GFAP:GP group were largely restricted to clusters 2, 5, and 9 (Fig. 2b, c). Together this highlights the effects of peripheral B cell depletion before the induction of LCMV GP expression in astrocytes and suggests that cluster 0 is most derived from peripherally recruited cells whereas clusters 2, 5, and 9 are not recirculating persisting in the CNS.

CNS infection generates long-lived brain-infiltrating ASCs that persist during autoimmunity

To further characterize B cell phenotypic diversity across all experimental conditions, we performed differential gene analysis, gene ontology, and gene set enrichment for each of the transcriptional clusters. Cluster 0 expressed genes related to interferon and antigen-presentation and was almost entirely composed of cells arising from GFAP:GP mice following TAM-mediated induction of GP and almost entirely absent in aCD20-GFAP:GP mice (Fig. 2c, d, supplementary Fig. 4a, 5, online resource). Cells from cluster 2 expressed genes related to germinal center B cells and contained comparable fractions of B cells from all four groups (Fig. 2c–e, supplementary Fig. 4b, online resource), representing a cluster that was likely induced by rLCMV-GP58 infection and was independent of GP neo-self antigen expression. Cells from clusters 4, 5 and 9 expressed genes related to ASCs (Fig. 2d, supplementary Fig. 4b, 5, online resource). Visualizing the expression of known B cell markers confirmed the unbiased transcriptional property of an ASC-phenotype of clusters 4, 5, and 9, as they expressed genes associated with antibody secretion programs (e.g., *Cd138* (*Sdc1*), *Taci* (*Tnfrsf13b*), *Xbp1*, *Slamf7, Nur77*) (Fig. 2e, supplementary Fig. 6, online resource). When performing B cell subset assignment we observed that cluster 4 was assigned the marginal zone (MZ) module. MZ B cells have been reported as precursors of PCs with additional evidence demonstrating that CD9, the main determinant of the MZ-module [49], is acquired by PCs during immune responses in a T cell-dependent fashion [78, 82]. Cells from GFAP:GP

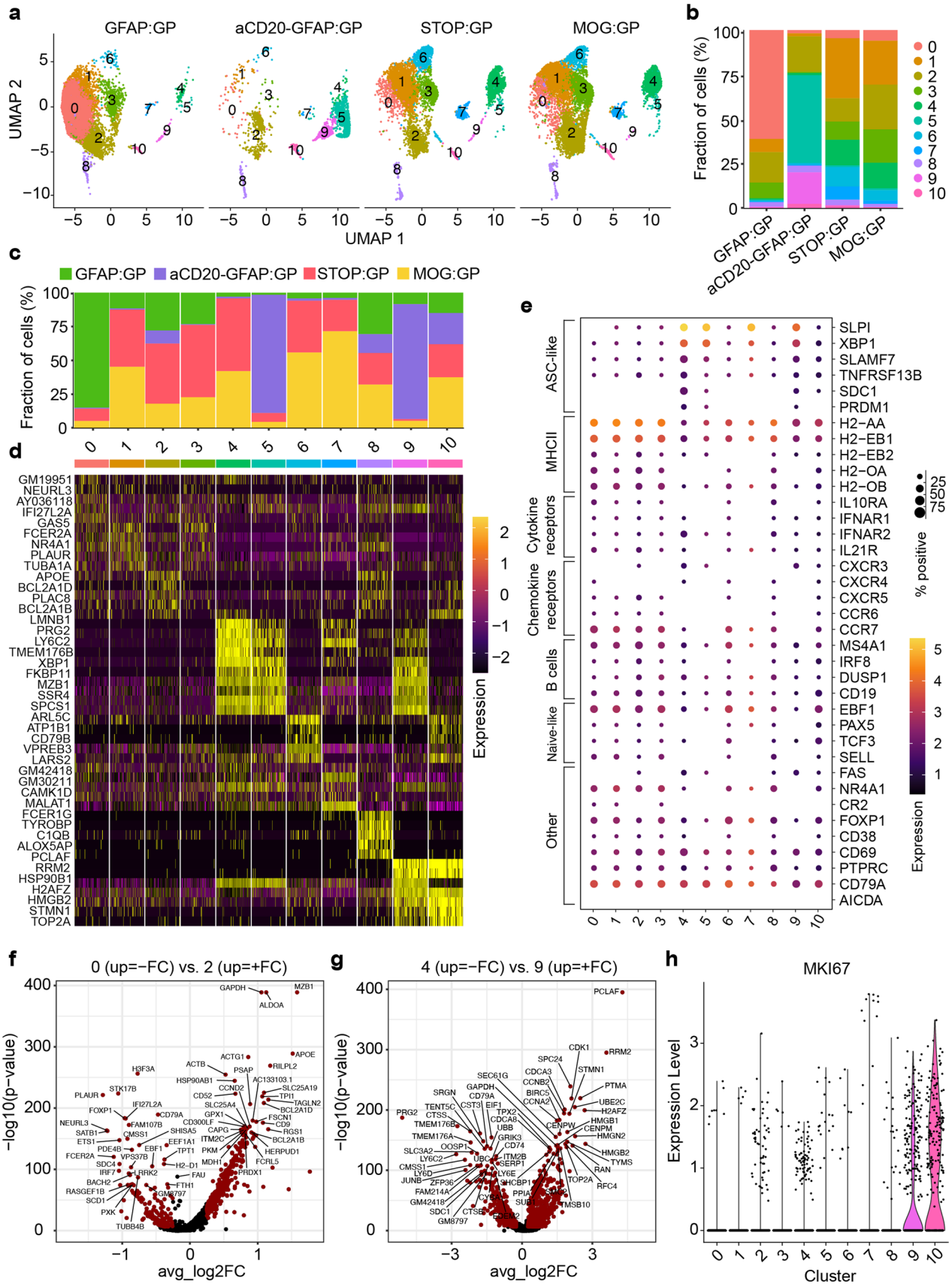
a
GFAP:GP
aCD20-GFAP:GP
STOP:GP
MOG:GP
UMAP 2
UMAP 1
b
Fraction of cells (%)
c
GFAP:GP aCD20-GFAP:GP STOP:GP MOG:GP
Fraction of cells (%)
d
Expression
e
ASC-like
MHCII
Cytokine receptors
Chemokine receptors
B cells
Naive-like
Other
% positive
Expression
f
0 (up=−FC) vs. 2 (up=+FC)
−log10(p−value)
avg_log2FC
g
4 (up=−FC) vs. 9 (up=+FC)
−log10(p−value)
avg_log2FC
h
MKI67
Expression Level
Cluster

◂**Fig. 2** Single-cell immune repertoire sequencing reveals heterogeneous populations of CNS B cells following infection and autoimmunity. **a** Uniform manifold approximate projection (UMAP) split by sample and colored by transcriptional cluster. **b** The fraction of cells in each transcriptional cluster separated by experimental group. **c** Distribution of experimental groups per transcriptional cluster. **d** Differentially expressed genes defining each cluster. **e** Gene expression levels of B cell markers separated by cluster membership (*x*-axis). The size of the dot corresponds to the percentage of cells expressing the given marker and the color indicates the mean expression per cell within each cluster. **f** Differentially expressed genes between clusters 0 and 2. Points in red indicate differentially expressed genes (adjusted *P* value < 0.01 and average log2 fold change (FC) > 0.25). 204 differentially expressed genes were upregulated in cluster 0 and 573 and in cluster 2. **g** Differentially expressed genes between clusters 4 and 9. 862 differentially expressed genes were upregulated in cluster 4 and 573 in cluster 9. **h** Normalized expression of *Mki67* separated by transcriptional cluster

mice expressed higher levels of genes associated with naive B cells and antigen-presentation (*Cd19*, *Sell*, *Ccr7,* and MHCII genes) (Fig. 2e, supplementary Fig. 6, online resource). The observed ASC and GC B cell phenotypes were in stark contrast to the transcriptional profiles of previously profiled CD19 + B cells populating the CNS in naive and aged mice which entirely lacked ASC-signatures [81]. Together, this implies that i.c. infection with rLCMV-GP58 induced ASCs in the brain that persist weeks following viral clearance (STOP:GP group) and that are maintained during autoimmunity (aCD20-GFAP:GP and MOG:GP groups).

As cluster 2 did not correspond to an ASC-phenotype yet remained after peripheral B cell depletion (~ 25% of all B cells from aCD20-GFAP:GP located in cluster 2 (Fig. 2b), we therefore calculated the differentially expressed genes between clusters 0 and 2 to shed light on those cells highly specific to the GFAP:GP group. This demonstrated that genes such as *Apoe, Mzb1, Ccnd2*, and genes related to *Bcl2*, were upregulated in cluster 2, whereas genes such as MHCII genes were relatively upregulated in cluster 0 (Fig. 2f, supplementary Fig. 4a, online resource). Together with the detected expression of *Fas* and *Cxcr3*, this suggests that TAM-driven induction of astrocytic GP recruits peripheral B cells that contribute in antigen-presentation and that B cells with upregulated germinal center markers persist in the CNS following peripheral B cell depletion.

Peripheral B cell depletion enriches proliferating ASCs upon neo-self-antigen induction

Having observed that ASC phenotypes were present across multiple clusters (4, 5, and 9) in a group-specific manner (Fig. 2a), we next questioned the underlying transcriptional heterogeneity of these subsets. While MOG:GP and STOP:GP mice contained cells located predominantly in cluster 4, the B cells isolated from aCD20-GFAP:GP mice were preferentially located in clusters 5 and 9 (Fig. 2b), suggesting that the inducible expression of LCMV GP by astrocytes further differentiated these cells. Of note, this ASC-phenotype is also visible in cells from GFAP:GP group, although likely masked due to massive recruitment of peripheral B cells that do not belong to clusters 4, 5 and 9. Expression of CD20 could still be detected within brain-derived cells from the aCD20-GFAP:GP group, albeit at a lower frequency (supplementary Fig. 7, online resource), suggesting that these cells were located behind the blood–brain barrier and thus inaccessible for depleting antibodies in the circulation. We next hypothesized that the B cells could have potentially adopted distinct transcriptional phenotypes due to the inflammatory milieu present following the induction and expression of GP by astrocytes. Performing differential gene expression analysis between clusters 4 and 9 revealed that cell-cycle and proliferation genes were enriched in cluster 9 (Fig. 2g), which paralleled the expression of the proliferation marker *Mki67* (Fig. 2h). Similarly, we observed cell proliferation associated genes, such as *Sub1* and *Fkbp11* [13, 61], enriched in cluster 5 relative to cluster 4 and less pronounced in cluster 9 (supplementary Fig. 8a, b, online resource), which further suggests a proliferative phenotype of the ASCs arising from aCD20-GFAP:GP brains.

Brain ASCs are clonally expanded and class-switched following viral infection and induction of autoimmunity

After having observed ASC expression profiles of B cells following infection and autoimmunity, we next questioned whether integrating antibody repertoire sequencing information would help elucidate the selection histories experienced by these B cells. We could recover full-length, paired-heavy-light chain antibody sequences for approximately 12,000 B cells, which resulted in a total of 8,187 clones across all experimental groups. Visualizing the fraction of clones that were supported by two or more unique cell barcodes demonstrated that clonal expansion was only detected in 17% of cells in the GFAP:GP group (Fig. 3a), supporting a model where peripheral B cells infiltrate in an antigen-independent manner. This was in stark contrast to the condition in which peripheral B cells were depleted, as clonal expansion was detected in 77% of clones (Fig. 3a). This high degree of clonal expansion in aCD20-GFAP:GP mice relative to other groups hinted towards a local antigen-reencounter event and local proliferation during the induction of GP following TAM administration, as baseline clonal expansion was detected in 45% of clones in STOP:GP mice (Fig. 3a).

To provide a more detailed description of these clonally expanded B cells, we next integrated repertoire features with transcriptional information. When overlaying

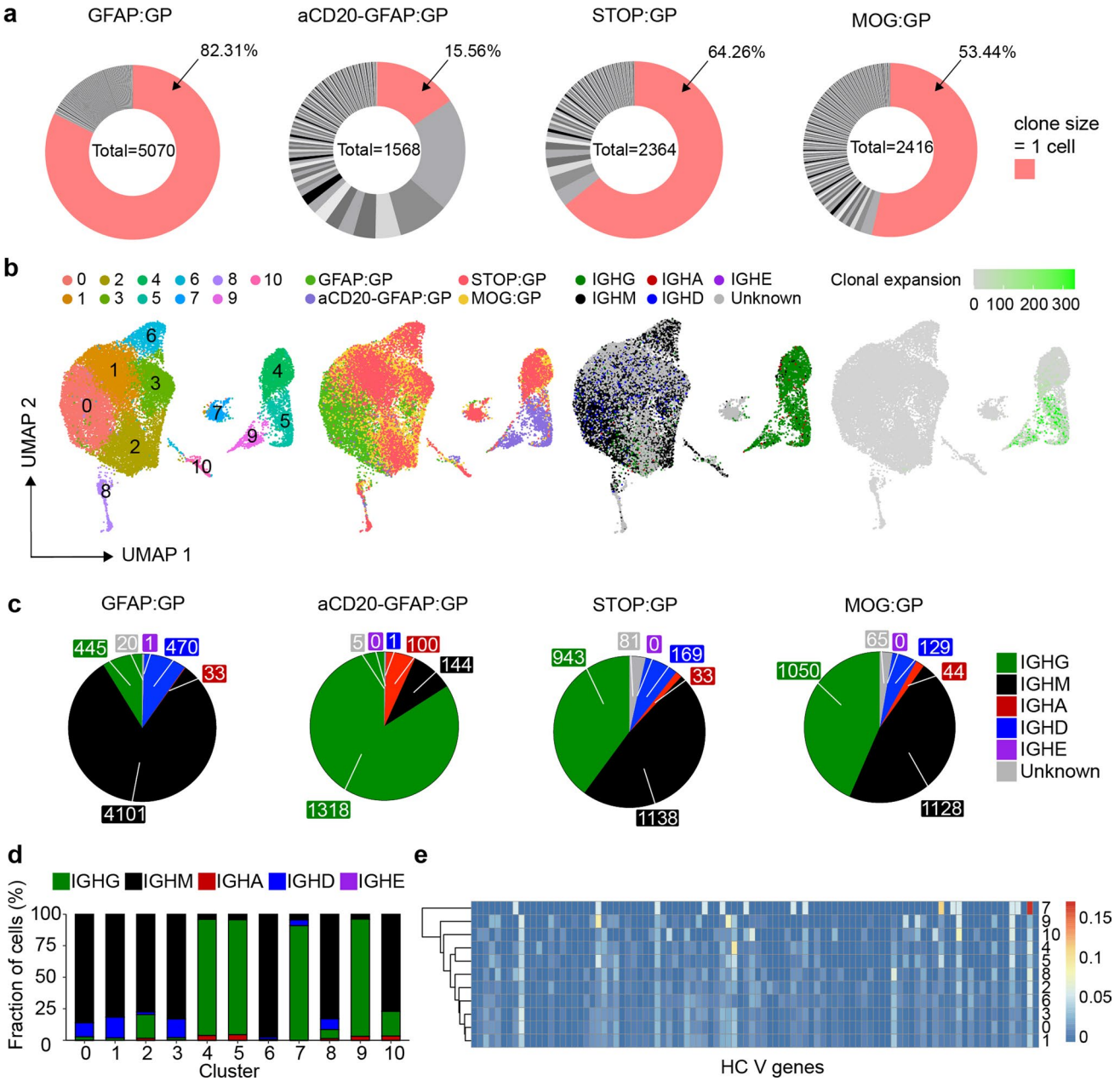

Fig. 3 Profiling the clonally expanded, class-switched antibody-secreting cells (ASCs) populating the brain following intracranial infection. **a** Distribution of clonal expansion for each experimental group. Each section corresponds to a unique clone and the size corresponds to the fraction of cells relative to the total repertoire. Red color highlights the fraction of clones containing 1 cell. The number in the center of the circle refers to the total number of recovered B cells. **b** Uniform manifold approximation projection (UMAP) depicting transcriptional cluster, group identity, antibody isotype, and clonal expansion for all recovered single-cells. Clonal expansion refers to the number of cells assigned to a single clone based on default clonotyping using Enclone. **c** Distribution of antibody isotype for all cells within each experimental group. **d** Distribution of antibody isotype for all cells within each transcriptional cluster. Cells with no isotype assigned (unknown) were removed. **e** Heavy chain clonal V gene usage across transcriptional clusters

antibody isotype onto the previously computed UMAP (Fig. 2a), we discovered that the ASCs like B cells in clusters 4, 5, and 9 were IgG-expressing and had higher levels of clonal expansion relative to the remaining IgM-dominant clusters (Fig. 3b). When quantifying isotype usage, we observed that GFAP:GP mice had the least amount of IgG, whereas this isotype represented the highest proportion for aCD20-GFAP:GP mice (Fig. 3c, d). In contrast, a considerable fraction (~50%) of B cells expressed IgG in STOP:GP and MOG:GP mice (Fig. 3c, d). The presence of these cells in MOG:GP mice shows that a population of clonally expanded, IgG-expressing ASCs cells persist in the

brain 7 weeks following i.c. viral infection despite persistent neo-self antigen expression. Having observed that certain B cell phenotypes were dominated by IgG-producing cells, we questioned whether these clusters preferentially employed certain germline genes, as this could hint towards shared antigen exposure. Indeed, hierarchical clustering demonstrated that ASC clusters (4, 5, 9) diverged from those clusters lacking the ASC phenotype (Fig. 3e), suggesting common selective pressures for those clonally expanded and IgG-expressing ASCs. Interestingly, this is in contrast to prior studies that have demonstrated IgA-secreting plasma cells in the meninges during homeostasis [24].

Clonally expanded and class-switched ASCs in the CNS are virus-specific and modulated by neo-self antigen induction

After characterizing the repertoire and transcriptional properties of clonally expanded ASCs cells, we investigated the functional properties of their antibodies. Visualizing the most expanded clones for each group demonstrated that despite GFAP:GP, STOP:GP, and MOG:GP groups having significant fractions of IgM-expressing cells (Fig. 3c, d), the vast majority of the most expanded clones were exclusively of the IgG isotype (supplementary Fig. 9a, online resource). Furthermore, we detected considerable somatic hypermutation within these expanded clones, as demonstrated by clonally related B cells expressing different antibodies (Fig. 4a). To discover the antigenic targets of these expanded IgG-producing B cells, we recombinantly expressed the antibodies from the most expanded clones for each group and interrogated antigen-specificity using enzyme-linked immunosorbent assay (ELISA) against a panel of LCMV, VSV, OVA and self-antigens (insulin and MOG). While no specificity was observed towards the self-antigens or OVA, we discovered that multiple clones arising from GFAP:GP, aCD20-GFAP:GP, and STOP:GP were specific to LCMV GP, whereas only LCMV nucleoprotein (NP) and no LCMV GP specificity was detected in the MOG:GP group (Fig. 4b, supplementary Fig. 9b, 10, online resource). While the GP- and NP-binding clones demonstrated distinct evolutionary histories, CDR3 sequence motifs, and germline gene usage, the majority of cells were located preferentially in clusters 4, 5 and 9 (Fig. 4c). Importantly, GP-specific clones from the GFAP:GP and aCD20-GFAP:GP groups were located in clusters 5 and 9, despite the relatively few cells occupying this cluster for the former group. The results of this functional validation strongly suggest that antigen-mediated reactivation of ASCs in the brain are common in both GFAP:GP and aCD20-GFAP:GP groups, but the high number of circulating B cells entering the CNS masked the detection of these cells in the former group. This was in contrast to the antigen-specific cells of STOP:GP and MOG:GP mice, where cells were preferentially located in cluster 4 (Fig. 4c, supplementary Fig. 9c, online resource), which corresponds to an ASC-cluster with relatively lower expression of proliferative genes and lower clonal expansion (Fig. 2g). Together, this further suggests that B cells in the CNS are capable of expansion in response to reencounters with cognate neo-self antigen.

Given that we only detected LCMV NP-specificity amongst the most expanded clones from the MOG:GP mice (Fig. 4b), we questioned whether the constitutive expression of GP by oligodendrocytes resulted in a deletion of GP specific B cells and thereby to B cell tolerance in the CNS. In contrast to brain-infiltrating B cells, ELISA on serum from infected MOG:GP mice (50 dpi) demonstrated reactivity to LCMV GP and LCMV NP (Fig. 5a), which was in accordance with previous results that MOG:GP mice did not induce peripheral tolerance in secondary lymphoid organs [57] and suggesting a tolerance specifically within the CNS. Given a recent report of local B cell tolerance to CNS antigens in the meninges [76], we profiled deeper into the expanded repertoire to uncover GP-specificity and investigated tolerance in secondary lymphoid organs occurring in our model. We therefore recombinantly produced an additional 10 clones from the expanded repertoire in the CNS of MOG:GP mice, which uncovered additional NP- but not GP-specific B cells (Fig. 5b). To provide further support for local CNS tolerance, we calculated the number of GP-specific clones (as determined in the other three experimental groups) present throughout the MOG:GP repertoire. Although minor clonal overlap was detected across all groups for both IgM/IgD and IgG isotypes when disregarding specificity (Fig. 5c), we did not detect any CDR3 sequences in the MOG:GP mice that corresponded to previously discovered GP-specific clones (Fig. 5d). Taken together, these findings support a model in which a constitutive expression of LCMV GP by glial cells induces localized elimination of self-reactive B cells and thus CNS tolerance.

Proliferating and class-switched ASCs are present across the brain and spinal cord following infection and induction of neo-self antigen

After confirming phenotypic and functional properties of CNS B cells, we next questioned where proliferating and class-switched ASCs were located within the CNS. We detected CD138 + IgG + cells within the brains of all experimental groups that were not present in naive mice (Fig. 6a). CD138 + IgG + cells co-expressing Ki67 could be detected in various anatomical regions of aCD20-GFAP:GP and GFAP:GP mice such as the meninges, the perivascular space and the parenchyma (Fig. 6b). Notably, we detected several instances of CD138 + IgG + Ki67 + cells located in clusters (Fig. 6c), in line with our hypothesis of antigen-mediated

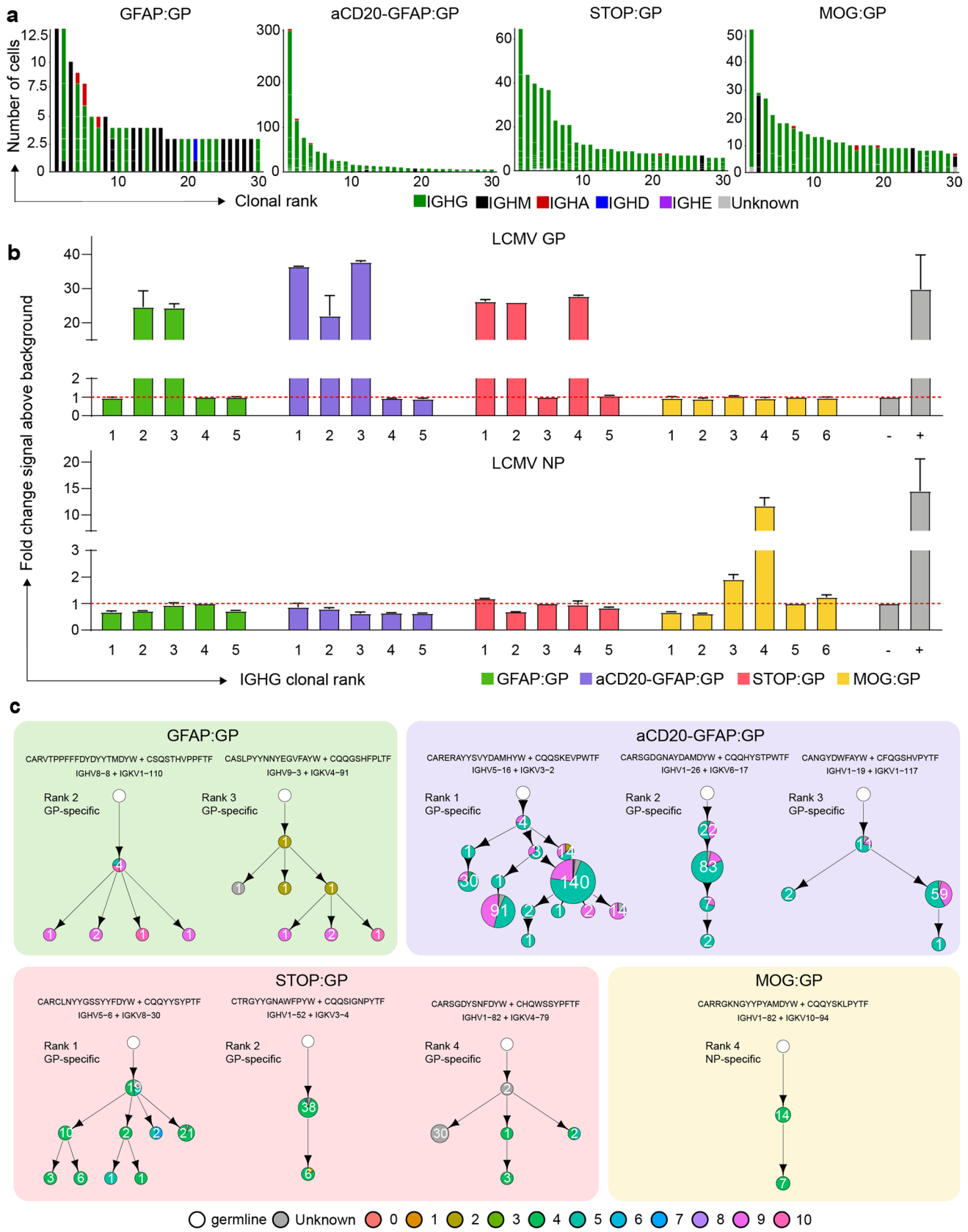
a
GFAP:GP
aCD20-GFAP:GP
STOP:GP
MOG:GP
Number of cells
Clonal rank
IGHG IGHM IGHA IGHD IGHE Unknown
b
LCMV GP
LCMV NP
Fold change signal above background
IGHG clonal rank
GFAP:GP aCD20-GFAP:GP STOP:GP MOG:GP
c
GFAP:GP
CARVTPPFFFDYDYYTMDYW + CSQSTHVPPFTF
IGHV8-8 + IGKV1-110
CASLPYYNNYEGVFAYW + CQQGSHFPLTF
IGHV9-3 + IGKV4-91
Rank 2
GP-specific
Rank 3
GP-specific
aCD20-GFAP:GP
CARERAYYSVYDAMHYW + CQQSKEVPWTF
IGHV5-16 + IGKV3-2
CARSGDGNAYDAMDYW + CQQHYSTPWTF
IGHV1-26 + IGKV6-17
CANGYDWFAYW + CFQGSHVPYTF
IGHV1-19 + IGKV1-117
Rank 1
GP-specific
Rank 2
GP-specific
Rank 3
GP-specific
STOP:GP
CARCLNYYGSSYYFDYW + CQQYYSYPTF
IGHV5-6 + IGKV8-30
CTRGYYGNAWFPYW + CQQSIGNPYTF
IGHV1-52 + IGKV3-4
CARSGDYSNFDYW + CHQWSSYPFTF
IGHV1-82 + IGKV4-79
Rank 1
GP-specific
Rank 2
GP-specific
Rank 4
GP-specific
MOG:GP
CARRGKNGYYPYAMDYW + CQQYSKLPYTF
IGHV1-82 + IGKV10-94
Rank 4
NP-specific
germline Unknown 0 1 2 3 4 5 6 7 8 9 10

◂**Fig. 4** The antigen specificity of clonally expanded and class-switched ASCs of the brain. **a** The relationship between the number of cells per clone and the number of clonally related antibody variants within the indicated clone. The thirty most expanded clones were selected per experimental group. Clone was determined by grouping those B cells containing identical CDRH3 + CDRL3 amino acid sequences. Variants within each clone are separated by a white line. Bar color refers to the isotype corresponding to the highest fraction of cells within the variant. **b** ELISA signal against lymphocytic choriomeningitis virus (LCMV) glycoprotein (GP) and nucleocapsid protein (NP). Clonal rank was determined within each group based on the highest number of cells within each clonotype. **c** Mutational networks of those specific clones. Nodes represent unique antibody variants (combined variable heavy [VH] and variable light [VL] chain nucleotide sequence) and edges demonstrate sequences with the smallest separation calculated by edit distance. Nodes are colored by transcriptional clusters. The size and label of the nodes indicate how many cells express each full-length antibody variant. Clone was determined by grouping those B cells containing identical CDRH3 + CDRL3 amino acid sequences. Only cells containing exactly one VH and VL were considered. The germline node represents the unmutated reference sequence determined by 10X Genomics cellranger. CDR3 Sequence motifs on top of each network and corresponding V genes. Color corresponds to biophysical properties

proliferation. In contrast, CD138 + IgG + cells from STOP:GP mice were almost entirely detected in the meninges and rarely in the perivascular space or the parenchyma. Finally, we observed several instances where two CD138 + IgG + cells appeared to maintain membrane connections (Fig. 6c), suggesting that cell division occurs locally within the CNS (Fig. 6c). Interestingly, we additionally observed that while the connected cells maintained expression of CD138 and IgG, only one of the two cells had detectable expression of Ki67 (Fig. 6c), which may indicate that ASCs undergo asymmetric cell division in the CNS. Taken together, our histological data supported our hypothesis that virus-specific B cells can be activated by encountering neo-self antigen in the CNS and adopt proliferative profiles.

Clonally expanded, class-switched, ASCs detected in the cerebrospinal fluid of human neurological diseases

We next questioned whether our experimental findings could be recapitulated in patients affected with inflammatory CNS conditions (Fig. 7a, supplementary Table 1, online resource). We therefore performed single-cell immune repertoire sequencing of the cerebrospinal fluid from three relapsing multiple sclerosis (RMS) patients. After filtering out T cells based on expression of CD3e, CD4 and CD8a expression, we performed unsupervised clustering and subsequently visualized the transcriptional landscape. This demonstrated the presence of multiple distinct B cell phenotypes shared across RMS patients (Fig. 7b). Consistent with our murine model, a distinct population of cerebrospinal fluid (CSF) B cells could be distinguished on the UMAP by ASC-associated genes, such as *SDC1 (CD138), TNFRSF99 (TACI), SLAMF7,* and *PRDM1 (BLIMP1)* (Fig. 7c, d). In accordance with previous studies [43], we saw approximately 20% of the ASC cluster expressing the proliferative marker *MKI67* (Fig. 7c). We next integrated immune receptor information onto the transcriptional landscape and observed that, in line with our murine model, the ASC clusters coincided with IgG expression (Fig. 7e). As we had discovered that clonally expanded, IgG-expressing ASCs were antigen-specific, we next questioned whether comparable levels of clonal expansion could be detected in the CSF of RMS patients. Overlaying expansion information for those clones supported by at least two distinct cell barcodes revealed that the vast majority of expanded clones were localized in the IgG-expressing ASC population (Fig. 7f). Given the high proportion of expanded clones located across all repertoires, we wondered whether somatic variants could be detected amongst the most expanded clones, similar as previously observed for the expanded IgG-expressing ASCs in our murine models. We therefore inferred phylogenetic networks for the most expanded clones (Fig. 7g), which indeed confirmed the presence of clonally related B cells expressing distinct antibodies within the CSF of all patients (Fig. 7h). In line with previous studies, we also observed the presence of the IgG1 isotype among the expanded ASCs, whereas the IgM isotype was expressed by other B cell populations (Fig. 7e, h) [43, 46, 74]. Taken together, these data suggest that the B-cell transcriptional properties in the CSF of RMS patients with relapsing disease share properties similar to those observed in our animal models.

Finally, we wondered if we can recapitulate our experimental findings of B cell phenotypes and patterns of clonal selection in the CSF of RMS patients. To this end, we furthermore compared the B cell populations in the CSF of patients with RMS to those with radiologically isolated syndrome (RIS), a preclinical stage of MS, by single-cell sequencing followed by integration of transcriptomic and repertoire features (supplementary Fig. 11, 12, Table 1, online resource). Unsupervised clustering demonstrated the presence of different B cell transcriptional signatures, among which three clusters (3, 4 and 5) were composed of IgG-class switched, expanded cells expressing ASC markers (supplementary Fig. 11a, b, c, online resource). Interestingly, we observed reduced expression of *Mki67* in the RIS group as compared to RMS both in the fraction of cells and in overall expression levels (supplementary Fig. 11d, e, online resource). We further observed lower B cell numbers per patient within the RIS group compared to MS patients, which is in line with previous reports of increased B cells in the CNS of MS patients compared to non-MS patients [28]. Next, we investigated the repertoire features of the B cells in the CSF from RIS patients, which

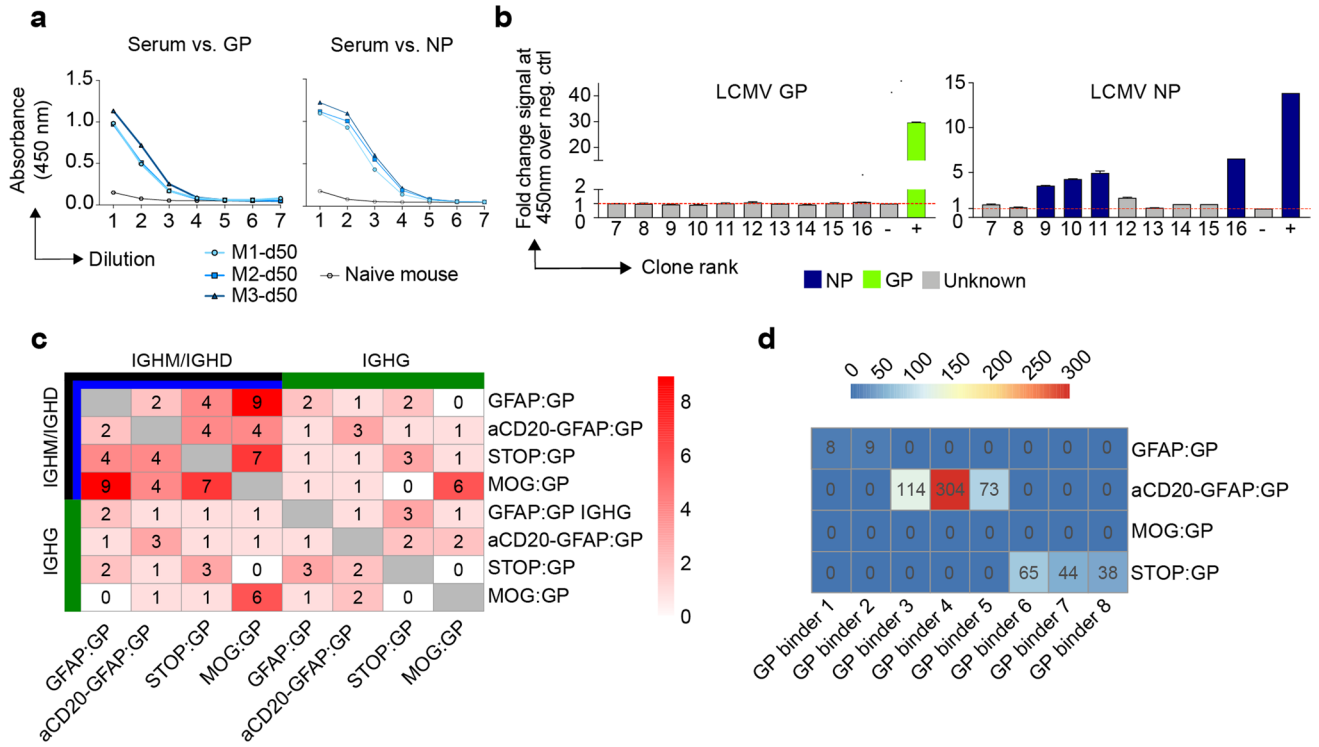

Fig. 5 Investigation of CNS-mediated local tolerance. **a** ELISA on fivefold pre-diluted serum (1:100) from uninfected mouse (naive) and infected MOG:GP mice (50 dpi) tested against lymphocytic choriomeningitis virus (LCMV) glycoprotein (GP) and nucleocapsid protein (NP). **b** ELISA signal against LCMV GP and LCMV NP for an additional 10 clones from the expanded repertoire of MOG:GP mice (Fig. 4a). **c** Number of IgM or IgG clones found in more than one repertoire. Clonotyping was performed based on those B cells containing identical HCDR3 + LCDR3 amino acid sequences. **d** Shared CDR3 amino acid GP-specific sequences across all conditions

demonstrated a lower magnitude of clonal expansion and class-switching compared to RMS patients (supplementary Fig. 12a, online resource). In contrast to the RMS patients, the most expanded clones from the RIS patients featured less intraclonal sequence variants after inferring phylogenetic networks (supplementary Fig. 12b, online resource). Visualizing the distribution of heavy chain V gene usage suggested preferential expression of the IGHV4 segment in both RIS and RMS patients (supplementary Fig. 12c, online resource), which is in line with previous reports [53, 54]. We also observed increased expression of the IGHV4 family within the ASC cluster in both RIS and RMS patients, whereas the V-gene distribution was more heterogeneous among non-ASCs B cells (supplementary Fig. 12c, online resource). Finally, we determined if certain VH-VL germline combinations were enriched in the ASC compartment, which suggested enrichment of the IGHV4-30–2/ IGKV1D-39 and IGHV3-7/IGKV1-5 pairing in the RMS group (supplementary Fig. 12d, online resource). Together, this comparison highlights unique phenotypic and repertoire fingerprints of B cells in the CSF of RMS patients which were distinct to RIS.

Discussion

B cells and their corresponding antibodies have been implicated in various chronic autoimmune disorders of the CNS. Here, we leveraged well-defined murine models of autoimmunity and infection to discover phenotypically and functionally diverse populations of B cells in the CNS. We discovered that clonally expanded and IgG-expressing populations of virus-specific ASCs persist in the CNS weeks after viral clearance. Furthermore, we show that these ASCs in the CNS reside in niches, but respond and proliferate following exposure to local autoantigens. Interestingly, this observation of IgG-expression is in contrast to prior studies that have demonstrated IgA-secreting plasma cells in the meninges during homeostasis [24]. Similar to the experimental models, we observed a population of class-switched, clonally expanded, somatically hypermutated, and proliferating ASCs in the CSF of RMS patients.

Consistent with the recently highlighted link between viral infection and MS [7], our data show that this ASC population described here represents expanded cells within the CNS that are potentially virus-specific and directed against antigens expressed in resident cells of the CNS. This is further supported by the observation that an expanded B cell

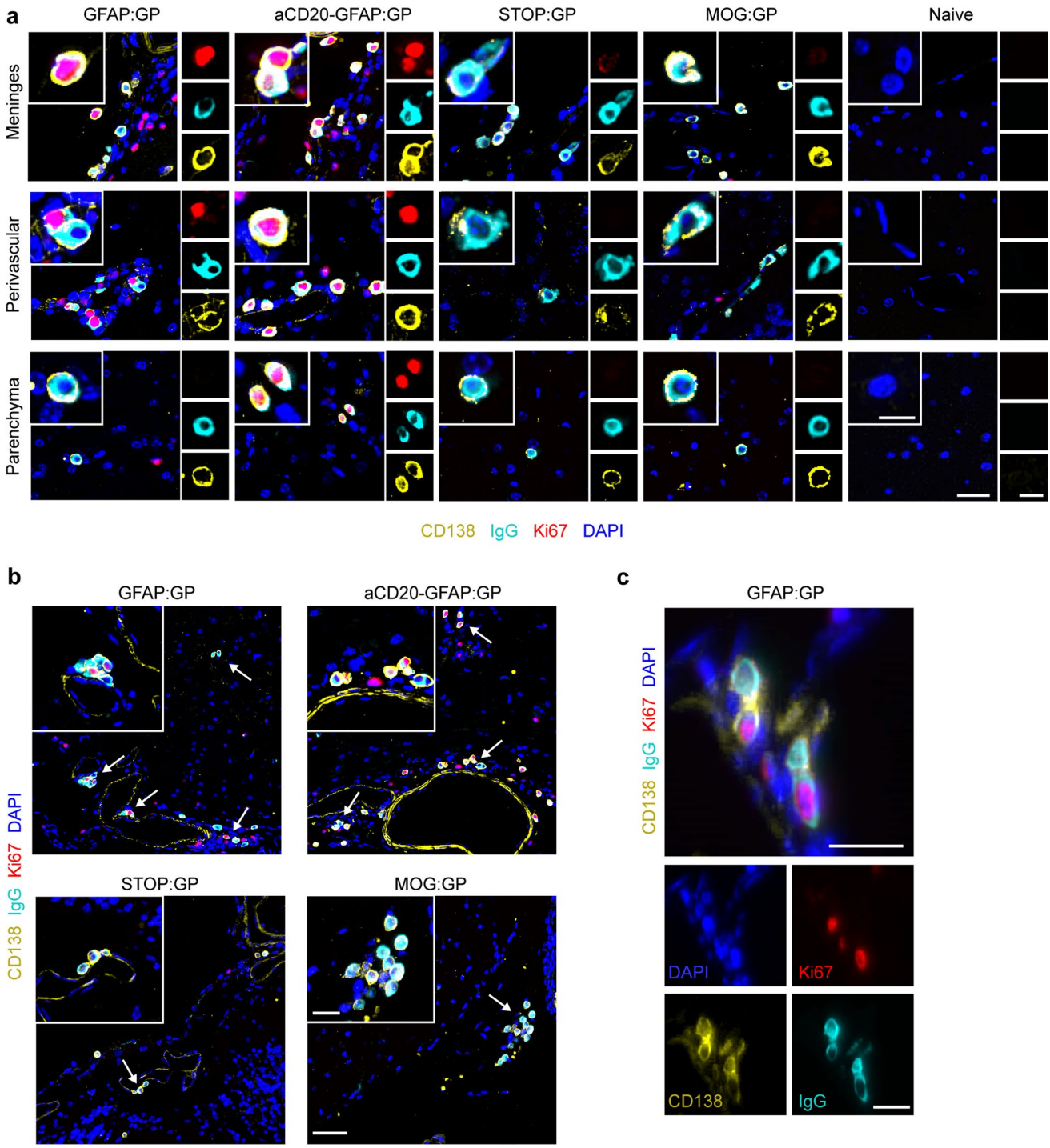

Fig. 6 Representative immunostainings for CD138, IgG, Ki67 and DAPI in brain sections of indicated groups. **a** CD138 + IgG + Ki67 ± are mostly located in meninges, perivascular space and parenchyma. Scale: 25 um. Inset: 10 um. **b** CD138 + IgG + Ki67 cells often localize in clusters (arrows). Scale: 50 um. Inset: 20 um. **c** CD138 + IgG + Ki67 + cells under cell division. Scale 20 um. One representative of at least two independent experiments is shown for (**a**–**c**)

clone in the CSF and blood of a RMS patient was recently shown to be cross-reactive against both Epstein–Barr virus (EBV) and the glial cell adhesion molecule GlialCAM [40]. It is thus likely that the phenotypic properties of this subset can be used to inform antigen specificity of the clonally expanded cells in human CSF in the context of neurological disorders which would substantiate the link between infection and neurological autoimmune disease. B cells are

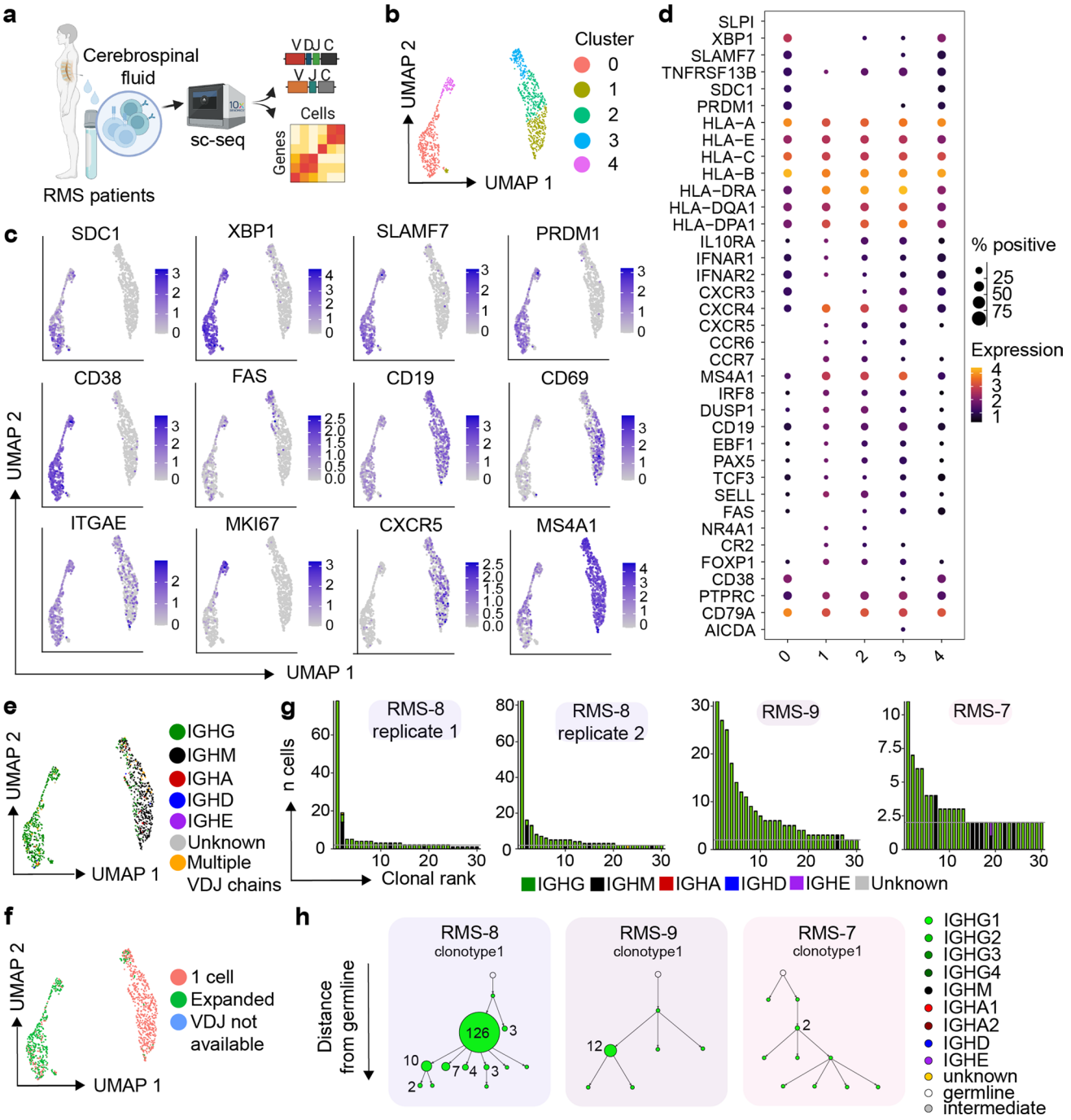

Fig. 7 Clonally expanded, class-switched, ASCs detected in the cerebrospinal fluid of multiple sclerosis (MS) patients. **a** Schematic overview for the analysis of B cells from RMS patients. **b** Uniform manifold approximate projection (UMAP) of human RMS patients colored by transcriptional cluster membership. **c** Gene expression of select genes UMAPs showing gene expression of selected B-cell genes. **d** Normalized expression of B-cell markers separated by cluster membership. **e** UMAP of human RMS patients colored by Isotype. **f** UMAP of human RMS patients colored by cell expansion. Expansion corresponds to those clones supported by more than one unique cell barcode. **g** Clonal frequencies for the 30 most expanded clones per experimental condition. Clones were determined according to 10×Genomics Cell Ranger's default clonotyping strategy. Clones containing 2 cells are highlighted with a horizontal gray line. Color corresponds to isotype as determined in the VDJ sequencing library. **h** Mutational network of the two most expanded clones per patient. Nodes represent unique antibody variants (combined variable heavy chain [VH] + variable light chain [VL] nucleotide sequences) and edges separate those sequences with the smallest edit distance. Node color corresponds to isotype identity. The size and label of the nodes indicate the number of cells expressing a single full-length antibody variant. Clones were determined according to 10×Genomics Cell Ranger's default clonotyping strategy and only those cells containing exactly one VH and VL chain were included. The germline node represents the unmutated reference sequence determined by 10×Genomics Cell Ranger

recruited in an antigen-independent manner under inflammatory conditions and can persist without necessarily exhibiting specificity for an antigen within the CNS, complicating the identification of pathophysiologically relevant B cells in inflammatory CNS conditions [72]. The approach presented here allows for the screening and identification of disease-relevant B cells and can constitute a new avenue for the development of targeted therapies in the context of CNS disorders. In addition, given that B cells efficiently present antigen and can activate cognate T cells [14], further profiling the specificity of the antigen presenting B cells discovered here could elucidate potential disease-relevant MHCII epitopes that would be presented to T cells.

Of note this subset of murine ASCs was entirely absent in the CNS of naive mice and in the widely used MOG_{35-55}- and $rMOG_{1-125}$-induced EAE mouse models [68, 81]. While minor clonal expansion of B cells was present in both naive and EAE conditions, the recovered B cells demonstrated either naive or memory B cell phenotypes and entirely lacked ASC gene signatures, class-switching, contemporary clonal variants, and expression of cell cycle and proliferation genes in contrast to MS patients as found in this study. Thus, our recently developed murine model as harnessed in the current work may not only serve as a valuable tool to profile and explore niches of CNS resident memory T cells, but also B cells with relevance to human neurological disease conditions. The formation and maintenance of resident memory B cells have been recently described in the lungs [3, 5, 71], with certain populations demonstrating ASC phenotypes upon reactivation [48]. Our observations that B cell populations persist in the CNS following aCD20 administration, suggests that at least a fraction of these cells may be tissue resident. This is in line with previous findings showing that B cells can be recruited and persist in an antigen-independent manner in the CNS [61, 72].

One further observation was the lack of B cells in the CNS reactive against LCMV GP when constitutively expressed as a neo-self antigen in oligodendrocytes. This suggests that the constant presence of neo-self antigen in the CNS results in deletional B cell tolerance preventing residence of autoantigen-specific B cells. The idea that deletional tolerance is occurring locally within the CNS and related niches following the recruitment of antigen-specific B cells is further supported by the fact that serum titers against the neo-self antigen remained unchanged. Such local tolerance mechanisms could potentially be related to hematopoietic niches within the meninges and skull that have been described as immune cell reservoirs and instruct B cells during development [11, 18]. Furthermore, it has been demonstrated that negative selection against CNS antigens occurs during B cell development within the meninges, although this investigation was restricted to MOG-specific B cells [76]. Mechanistically, CSF-mediated cross-talk between the brain, meninges, and skull bone marrow niches may contribute to the distribution and accessibility of the neo-self antigen locally within the CSF. This would be in line with recent findings showing that intra cisterna magna injections drain to local skull bone marrow niches but not those present in the tibia [50], which would further prevent the induction of peripheral tolerance. To what extent and how such tolerance mechanisms become dysfunctional in human chronic autoimmune diseases will be an important task to resolve in future work.

Our study has significant implications for the reactivation, expansion and tolerance of virus-specific and autoreactive B cells in the CNS, but there remain several limitations that prompt future investigations. Firstly, while B cells from the CNS were sorted using the CD19 marker among others, histological quantification was performed using mouse pan B cell marker B220 based on its reliability for immunohistochemical staining on PFA-fixed tissues [9, 20, 42, 45, 47, 58, 75, 79]. However, it is possible that CD19 and B220 may not exactly overlap although we expect similar trends based on our sequencing results and additional histology measuring the ASC population. Second, the patients included in this study were limited exclusively to patients with RMS and RIS. Further studies with larger cohorts, including different MS subtypes and further control groups would be needed to inform us about the specific role of observed B-cells in the pathophysiology and inform us about the recruitment, reactivation, and differentiation mechanisms of these cells in the various human disease contexts. Third, the B cells in the CSF of analyzed patients only partially represent the total B-cell population expected to be present in the CNS, and may thus not reflect the full spectrum of B phenotypes and representations found in the CNS tissue as investigated in the murine brains. Future studies integrating single-cell immune repertoire sequencing and spatial transcriptomics, for example, are important to understand whether anatomical location influences the clonality and biophysical properties of neoantigen-specific antibodies. Finally, an interesting future endeavor would be comparing transcriptional, repertoire, and biophysical properties of antibodies, between our murine models with CNS B cells from patients with viral encephalitis. Such comparisons will help to better understand the translational impact of our murine models and may offer specific biomarkers of autoreactive B cells.

Overall, our study highlights the clonal dynamics of B cells populating the CNS during infection and autoimmunity in experimental models and human disease conditions. It further emphasizes that B cells can undergo clonal selection and respond to autoantigens expressed in the CNS and it delineates the transcriptional characteristics of ASC populations that can be used to determine the antigen origin of B cell responses taken place within the CNS. Finally, our study

serves as a starting point to unravel the poorly understood underpinnings of B cell dysregulation in chronic inflammatory CNS diseases.

Supplementary Information The online version contains supplementary material available at https://doi.org/10.1007/s00401-023-02537-5.

Acknowledgements We acknowledge and thank Dr. Christian Beisel, Elodie Burcklen, and Ina Nissen at the ETH Zurich D-BSSE Genomics Facility Basel for excellent support and assistance. We also thank Gregory Schneiter for excellent experimental support.

Author contributions AY, DM, EB, AO and STR conceived the project and supervised this study. AA, RD, IV, IW, RK, DS, MMC, TSC, KLH, NP, NF, GS, AM, MP, BG, AG, AP, SF, HT, VK, LAG, KD and AY performed experiments; AA, AY, IV, RD, MMC, MK and TSC participated in the data analysis. All of the authors wrote, revised or discussed the manuscript.

Funding Open access funding provided by Swiss Federal Institute of Technology Zurich. This work was supported by the European Research Council Starting Grant 679403 (to STR), ETH Zurich Research Grants (to STR and AO), an ETH Seed Grant (AY) and support from the "la Caixa" Foundation (ID 100010434, fellowship code: LCF/BQ/EU20/11810041) to MMC. DM is supported by the Swiss National Science Foundation (310030B_201271 and 310030_185321) and the ERC (865026). This study was further supported by the German Research Foundation: DO 420/7-1 (KD and EB), EXC 2145 (SyNergy) – ID 390857198 (LAG, KD and EB), and by the DFG Research Infrastructure NGS_CC (project 407495230) as part of the Next Generation Sequencing Competence Network (project 423957469). NGS was carried out at the Competence Centre for Genomic Analysis (Kiel).

Availability of data and materials Sequencing data has been deposited under accession number E-MTAB-12590 and PRJNA925519 in the European Bioinformatics Institute and NCBI BioProject, respectively. All relevant data generated and analyzed in this study are available in this manuscript, online supplementary information or upon request.

Declarations

Conflict of interest There are no competing interests.

Ethical approval The study was approved by the local ethics committee of the Ludwig-Maximilian University Munich (project nos. 163-16 and 18-419), and written informed consent was granted by all participants included in the study.

Open Access This article is licensed under a Creative Commons Attribution 4.0 International License, which permits use, sharing, adaptation, distribution and reproduction in any medium or format, as long as you give appropriate credit to the original author(s) and the source, provide a link to the Creative Commons licence, and indicate if changes were made. The images or other third party material in this article are included in the article's Creative Commons licence, unless indicated otherwise in a credit line to the material. If material is not included in the article's Creative Commons licence and your intended use is not permitted by statutory regulation or exceeds the permitted use, you will need to obtain permission directly from the copyright holder. To view a copy of this licence, visit http://creativecommons.org/licenses/by/4.0/.

References

1. Agrafiotis A, Neumeier A, Hong KH, Chowdhury T, Ehling R, Kuhn R t al (2022) Generation of a single-cell B cell atlas of antibody repertoires and transcriptomes to identify signatures associated with antigen-specificity. bioRxiv. https://doi.org/10.1101/2021.11.09.467876
2. Agrawal S, Anderson P, Durbeej M, van Rooijen N, Ivars F, Opdenakker G et al (2006) Dystroglycan is selectively cleaved at the parenchymal basement membrane at sites of leukocyte extravasation in experimental autoimmune encephalomyelitis. J Exp Med 203:1007–1019
3. Allie SR, Bradley JE, Mudunuru U, Schultz MD, Graf BA, Lund FE et al (2019) The establishment of resident memory B cells in the lung requires local antigen encounter. Nat Immunol 20:97–108
4. Allie SR, Randall TD (2020) Resident memory B cells. Viral Immunol 33:282–293
5. Barker KA, Etesami NS, Shenoy AT, Arafa EI, Lyon de Ana C, Smith NM et al (2021) Lung-resident memory B cells protect against bacterial pneumonia. J Clin Invest. https://doi.org/10.1172/JCI141810
6. Barr TA, Shen P, Brown S, Lampropoulou V, Roch T, Lawrie S et al (2012) B cell depletion therapy ameliorates autoimmune disease through ablation of IL-6-producing B cells. J Exp Med 209:1001–1010
7. Bjornevik K, Cortese M, Healy BC, Kuhle J, Mina MJ, Leng Y et al (2022) Longitudinal analysis reveals high prevalence of Epstein-Barr virus associated with multiple sclerosis. Science 375:296–301
8. Boronat A, Gelfand JM, Gresa-Arribas N, Jeong H-Y, Walsh M, Roberts K et al (2013) Encephalitis and antibodies to dipeptidyl-peptidase-like protein-6, a subunit of Kv4.2 potassium channels. Ann Neurol 73:120–128
9. Brand RM, Friedrich V, Diddens J, Pfaller M, Romana de Franchis F, Radbruch H et al (2021) Anti-CD20 depletes meningeal B cells but does not halt the formation of meningeal ectopic lymphoid tissue. Neurol Neuroimmunol Neuroinflamm. https://doi.org/10.1212/NXI.0000000000001012
10. Brilot F, Dale RC, Selter RC, Grummel V, Kalluri SR, Aslam M et al (2009) Antibodies to native myelin oligodendrocyte glycoprotein in children with inflammatory demyelinating central nervous system disease. Ann Neurol 66:833–842
11. Brioschi S, Wang W-L, Peng V, Wang M, Shchukina I, Greenberg ZJ et al (2021) Heterogeneity of meningeal B cells reveals a lymphopoietic niche at the CNS borders. Science. https://doi.org/10.1126/science.abf9277
12. Carbone FR (2015) Tissue-resident memory T cells and fixed immune surveillance in nonlymphoid organs. J Immunol 195:17–22
13. Chakravarthi BVSK, Goswami MT, Pathi SS, Robinson AD, Cieślik M, Chandrashekar DS et al (2016) MicroRNA-101 regulated transcriptional modulator SUB1 plays a role in prostate cancer. Oncogene 35:6330–6340
14. Chen X, Jensen PE (2008) The role of B lymphocytes as antigen-presenting cells. Arch Immunol Ther Exp 56:77–83
15. Chitnis T, Weiner HL (2017) CNS inflammation and neurodegeneration. J Clin Invest 127:3577–3587
16. Clark RA (2015) Resident memory T cells in human health and disease. Sci Transl Med 7:269rv1
17. Csepregi L, Ehling RA, Wagner B, Reddy ST (2020) Immune literacy: reading, writing, and editing adaptive immunity. iScience 23:101519
18. Cugurra A, Mamuladze T, Rustenhoven J, Dykstra T, Beroshvili G, Greenberg ZJ et al (2021) Skull and vertebral bone marrow are

myeloid cell reservoirs for the meninges and CNS parenchyma. Science. https://doi.org/10.1126/science.abf7844
19. Dalakas MC, Alexopoulos H, Spaeth PJ (2020) Complement in neurological disorders and emerging complement-targeted therapeutics. Nat Rev Neurol 16:601–617
20. Dang AK, Tesfagiorgis Y, Jain RW, Craig HC, Kerfoot SM (2015) Meningeal infiltration of the spinal cord by non-classically activated B cells is associated with chronic disease course in a spontaneous B cell-dependent model of CNS autoimmune disease. Front Immunol. https://doi.org/10.3389/fimmu.2015.00470
21. Dijkgraaf FE, Matos TR, Hoogenboezem M, Toebes M, Vredevoogd DW, Mertz M et al (2019) Tissue patrol by resident memory CD8+ T cells in human skin. Nat Immunol 20:756–764
22. Flatz L, Bergthaler A, de la Torre JC, Pinschewer DD (2006) Recovery of an arenavirus entirely from RNA polymerase I/II-driven cDNA. Proc Natl Acad Sci U S A 103:4663–4668
23. Fillatreau S, Sweenie CH, McGeachy MJ, Gray D, Anderton SM (2002) B cells regulate autoimmunity by provision of IL-10. Nat Immunol 3:944–950
24. Fitzpatrick Z, Frazer G, Ferro A, Clare S, Bouladoux N, Ferdinand J et al (2020) Gut-educated IgA plasma cells defend the meningeal venous sinuses. Nature 587:472–476
25. Frebel H, Richter K, Oxenius A (2010) How chronic viral infections impact on antigen-specific T-cell responses. Eur J Immunol 40:654–663
26. Ghersi-Egea J-F, Strazielle N, Catala M, Silva-Vargas V, Doetsch F, Engelhardt B (2018) Molecular anatomy and functions of the choroidal blood–cerebrospinal fluid barrier in health and disease. Acta Neuropathol 135:337–361
27. Gray JI, Farber DL (2022) Tissue-resident immune cells in humans. Annu Rev Immunol. https://doi.org/10.1146/annurev-immunol-093019-112809
28. Han S, Lin YC, Wu T, Salgado AD, Mexhitaj I, Wuest SC et al (2014) Comprehensive immunophenotyping of cerebrospinal fluid cells in patients with neuroimmunological diseases. J Immunol 192:2551–2563
29. Häusser-Kinzel S, Weber MS (2019) The role of B cells and antibodies in multiple sclerosis, neuromyelitis optica, and related disorders. Front Immunol 10:201
30. Hiltensperger M, Beltrán E, Kant R, Tyystjärvi S, Lepennetier G, Domínguez Moreno H, Bauer IJ, Grassmann S, Jarosch S, Schober K, Buchholz VR, Kenet S, Gasperi C, Öllinger R, Rad R, Muschaweckh A, Sie C, Aly L, Knier B, Garg G, Afzali AM, Gerdes LA, Kümpfel T, Franzenburg S, Kawakami N, Hemmer B, Busch DH, Misgeld T, Dornmair K, Korn T (2021) Skin and gut imprinted helper T cell subsets exhibit distinct functional phenotypes in central nervous system autoimmunity. Nat Immunol 22:880–892
31. Hirrlinger PG, Scheller A, Braun C, Hirrlinger J, Kirchhoff F (2006) Temporal control of gene recombination in astrocytes by transgenic expression of the tamoxifen-inducible DNA recombinase variant CreERT2. Glia 54:11–20
32. Horns F, Dekker CL, Quake SR (2020) Memory B cell activation, broad anti-influenza antibodies, and bystander activation revealed by single-cell transcriptomics. Cell Rep 30:905-913.e6
33. Hövelmeyer N, Hao Z, Kranidioti K, Kassiotis G, Buch T, Frommer F et al (2005) Apoptosis of oligodendrocytes via Fas and TNF-R1 is a key event in the induction of experimental autoimmune encephalomyelitis. J Immunol 175:5875–5884
34. Jain RW, Yong VW (2021) B cells in central nervous system disease: diversity, locations and pathophysiology. Nat Rev Immunol. https://doi.org/10.1038/s41577-021-00652-6
35. Jarius S, Paul F, Franciotta D, Waters P, Zipp F, Hohlfeld R et al (2008) Mechanisms of disease: aquaporin-4 antibodies in neuromyelitis optica. Nat Clin Pract Neurol 4:202–214
36. Jiang X, Clark RA, Liu L, Wagers AJ, Fuhlbrigge RC, Kupper TS (2012) Skin infection generates non-migratory memory CD8+ TRM cells providing global skin immunity. Nature 483:227–231
37. Kallert SM, Darbre S, Bonilla WV, Kreutzfeldt M, Page N, Müller P, Kreuzaler M, Lu M, Favre S, Kreppel F, Löhning M, Luther SA, Zippelius A, Merkler D, Pinschewer DD (2017) Replicating viral vector platform exploits alarmin signals for potent CD8 T cell-mediated tumour immunotherapy. Nat Commun 8:15327
38. Korotkevich G, Sukhov V, Budin N, Shpak B, Artyomov MN, Sergushichev A (2016) Fast gene set enrichment analysis. bioRxiv
39. Krumbholz M, Derfuss T, Hohlfeld R, Meinl E (2012) B cells and antibodies in multiple sclerosis pathogenesis and therapy. Nat Rev Neurol 8:613–623
40. Lanz TV, Brewer RC, Ho PP, Moon J-S, Jude KM, Fernandez D et al (2022) Clonally expanded B cells in multiple sclerosis bind EBV EBNA1 and GlialCAM. Nature. https://doi.org/10.1038/s41586-022-04432-7
41. Lee DSW, Rojas OL, Gommerman JL (2021) B cell depletion therapies in autoimmune disease: advances and mechanistic insights. Nat Rev Drug Discov 20:179–199
42. Lehmann-Horn K, Sagan SA, Winger RC, Spencer CM, Bernard CCA, Sobel RA et al (2016) CNS accumulation of regulatory B cells is VLA-4-dependent. Neurol Neuroimmunol Neuroinflamm 3:e212
43. Lindeman I, Polak J, Qiao S-W, Holmøy T, Høglund RA, Vartdal F et al (2022) Stereotyped B-cell responses are linked to IgG constant region polymorphisms in multiple sclerosis. Eur J Immunol 52:550–565
44. Li R, Patterson KR, Bar-Or A (2018) Reassessing B cell contributions in multiple sclerosis. Nat Immunol 19:696–707
45. Liu Y, Luo J, Carlsson MA, Nässel DR (2015) Serotonin and insulin-like peptides modulate leucokinin-producing neurons that affect feeding and water homeostasis in Drosophila. J Comp Neurol 523:1840–1863
46. Lossius A, Tomescu-Baciu A, Holmøy T, Vedeler CA, Røsjø E, Lorentzen ÅR et al (2017) Selective intrathecal enrichment of G1m1-positive B cells in multiple sclerosis. Ann Clin Transl Neurol 4:756–761
47. Louveau A, Smirnov I, Keyes TJ, Eccles JD, Rouhani SJ, Peske JD et al (2016) Corrigendum: structural and functional features of central nervous system lymphatic vessels. Nature 533:278
48. MacLean AJ, Richmond N, Koneva L, Attar M, Medina CAP, Thornton EE et al (2022) Secondary influenza challenge triggers resident memory B cell migration and rapid relocation to boost antibody secretion at infected sites. Immunity. https://doi.org/10.1016/j.immuni.2022.03.003
49. Mathew NR, Jayanthan JK, Smirnov IV, Robinson JL, Axelsson H, Nakka SS et al (2021) Single-cell BCR and transcriptome analysis after influenza infection reveals spatiotemporal dynamics of antigen-specific B cells. Cell Rep 35:109286
50. Mazzitelli JA, Smyth LCD, Cross KA, Dykstra T, Sun J, Du S et al (2022) Cerebrospinal fluid regulates skull bone marrow niches via direct access through dural channels. Nat Neurosci. https://doi.org/10.1038/s41593-022-01029-1
51. Meinl E, Krumbholz M, Hohlfeld R (2006) B lineage cells in the inflammatory central nervous system environment: migration, maintenance, local antibody production, and therapeutic modulation. Ann Neurol 59:880–892
52. Neumeier D, Pedrioli A, Genovese A, Sandu I, Ehling R, Hong K-L et al (2021) Profiling the specificity of clonally expanded plasma cells during chronic viral infection by single-cell analysis. Eur J Immunol. https://doi.org/10.1002/eji.202149331
53. Owens GP, Kannus H, Burgoon MP, Smith-Jensen T, Devlin ME, Gilden DH (1998) Restricted use of VH4 Germline segments in an acute multiple sclerosis brain. Ann Neurol 43:236–243

54. Owens GP, Winges KM, Ritchie AM, Edwards S, Burgoon MP, Lehnhoff L et al (2007) V_H4 gene segments dominate the intrathecal humoral immune response in multiple sclerosis. J Immunol 179:6343–6351
55. Owens T, Bechmann I, Engelhardt B (2008) Perivascular spaces and the two steps to neuroinflammation. J Neuropathol Exp Neurol 67:1113–1121
56. Page N, Klimek B, De Roo M, Steinbach K, Soldati H, Lemeille S et al (2019) Expression of the DNA-binding factor TOX promotes the encephalitogenic potential of microbe-induced autoreactive CD8 T cells. Immunity 50:763
57. Page N, Lemeille S, Vincenti I, Klimek B, Mariotte A, Wagner I et al (2021) Persistence of self-reactive CD8+ T cells in the CNS requires TOX-dependent chromatin remodeling. Nat Commun 12:1009
58. Pollok K, Mothes R, Ulbricht C, Liebheit A, Gerken JD, Uhlmann S et al (2017) The chronically inflamed central nervous system provides niches for long-lived plasma cells. Acta Neuropathol Commun 5:88
59. Prinz M, Priller J (2017) The role of peripheral immune cells in the CNS in steady state and disease. Nat Neurosci 20:136–144
60. Prüss H (2021) Autoantibodies in neurological disease. Nat Rev Immunol 21:798–813
61. Qiu L, Liu H, Wang S, Dai X-H, Shang J-W, Lian X-L et al (2021) FKBP11 promotes cell proliferation and tumorigenesis via p53-related pathways in oral squamous cell carcinoma. Biochem Biophys Res Commun 559:183–190
62. Ramesh A, Schubert RD, Greenfield AL, Dandekar R, Loudermilk R, Sabatino JJ Jr et al (2020) A pathogenic and clonally expanded B cell transcriptome in active multiple sclerosis. Proc Natl Acad Sci U S A 117:22932–22943
63. Robinson MD, McCarthy DJ, Smyth GK (2010) edgeR: a Bioconductor package for differential expression analysis of digital gene expression data. Bioinformatics 26(1):139–40. https://doi.org/10.1093/bioinformatics/btp616
64. Sabatino JJ Jr, Pröbstel A-K, Zamvil SS (2019) B cells in autoimmune and neurodegenerative central nervous system diseases. Nat Rev Neurosci 20:728–745
65. Satija R, Farrell JA, Gennert D, Schier AF, Regev A (2015) Spatial reconstruction of single-cell gene expression data. Nat Biotechnol 33:495–502
66. Schenkel JM, Masopust D (2014) Tissue-resident memory T cells. Immunity 41:886–897
67. Schwartz M, Kipnis J, Rivest S, Prat A (2013) How do immune cells support and shape the brain in health, disease, and aging? J Neurosci 33:17587–17596
68. Shlesinger D, Hong K-L, Shammas G, Page N, Sandu I, Agrafiotis A et al (2022) Single-cell immune repertoire sequencing of B and T cells in murine models of infection and autoimmunity. bioRxiv. https://doi.org/10.1101/2022.02.07.479381
69. Smets I, Titulaer MJ (2022) Antibody therapies in autoimmune encephalitis. Neurotherapeutics. https://doi.org/10.1007/s13311-021-01178-4
70. Steinbach K, Vincenti I, Kreutzfeldt M, Page N, Muschaweckh A, Wagner I et al (2016) Brain-resident memory T cells represent an autonomous cytotoxic barrier to viral infection. J Exp Med 213:1571–1587
71. Tan H-X, Juno JA, Esterbauer R, Kelly HG, Wragg KM, Konstandopoulos P et al (2022) Lung-resident memory B cells established after pulmonary influenza infection display distinct transcriptional and phenotypic profiles. Sci Immunol 7:eabf5314
72. Tesfagiorgis Y, Zhu SL, Jain R, Kerfoot SM (2017) Activated B cells participating in the anti-myelin response are excluded from the inflamed central nervous system in a model of autoimmunity that allows for B cell recognition of autoantigen. J Immunol 199:449–457
73. Urban SL, Jensen IJ, Shan Q, Pewe LL, Xue H-H, Badovinac VP et al (2020) Peripherally induced brain tissue-resident memory CD8+ T cells mediate protection against CNS infection. Nat Immunol 21:938–949
74. Vartdal F, Vandvik B (1983) Multiple sclerosis: subclasses of intrathecally synthesized IgG and measles and varicella zoster virus IgG antibodies. Clin Exp Immunol 54:641–647
75. Vincenti I, Page N, Steinbach K, Yermanos A, Lemeille S, Nunez N et al (2022) Tissue-resident memory CD8+ T cells cooperate with CD4+ T cells to drive compartmentalized immunopathology in the CNS. Sci Transl Med 14:eabl6058
76. Wang Y, Chen D, Xu D, Huang C, Xing R, He D et al (2021) Early developing B cells undergo negative selection by central nervous system-specific antigens in the meninges. Immunity 54:2784-2794.e6
77. Wilson EH, Weninger W, Hunter CA (2010) Trafficking of immune cells in the central nervous system. J Clin Invest 120:1368–1379
78. Won W-J, Kearney JF (2002) CD9 is a unique marker for marginal zone B cells, B1 cells, and plasma cells in mice. J Immunol 168:5605–5611
79. Wu L, Li N, Zhang M, Xue S-L, Cassady K, Lin Q et al (2015) MHC-mismatched mixed chimerism augments thymic regulatory T-cell production and prevents relapse of EAE in mice. Proc Natl Acad Sci USA 112:15994–15999
80. Yermanos A, Agrafiotis A, Kuhn R, Robbiani D, Yates J, Papadopoulou C et al (2021) Platypus: an open-access software for integrating lymphocyte single-cell immune repertoires with transcriptomes. NAR Genom Bioinform. https://doi.org/10.1093/nargab/lqab023
81. Yermanos A, Neumeier D, Sandu I, Borsa M, Waindok AC, Merkler D et al (2021) Single-cell immune repertoire and transcriptome sequencing reveals that clonally expanded and transcriptionally distinct lymphocytes populate the aged central nervous system in mice. Proc R Soc B: Biol Sci 288:20202793
82. Yoon S-O, Zhang X, Lee IY, Spencer N, Vo P, Choi YS (2013) CD9 is a novel marker for plasma cell precursors in human germinal centers. Biochem Biophys Res Commun 431:41–46

Publisher's Note Springer Nature remains neutral with regard to jurisdictional claims in published maps and institutional affiliations.

Authors and Affiliations

Andreas Agrafiotis[1,2] · Raphael Dizerens[1] · Ilena Vincenti[3] · Ingrid Wagner[3] · Raphael Kuhn[1] · Danielle Shlesinger[1] · Marcos Manero-Carranza[1] · Tudor-Stefan Cotet[1] · Kai-Lin Hong[1] · Nicolas Page[3] · Nicolas Fonta[3] · Ghazal Shammas[3] · Alexandre Mariotte[3] · Margot Piccinno[3] · Mario Kreutzfeldt[3,9] · Benedikt Gruntz[1] · Roy Ehling[1] · Alessandro Genovese[2] · Alessandro Pedrioli[2] · Andreas Dounas[4] · Sören Franzenburg[5] · Hayrettin Tumani[10] · Tania Kümpfel[6,7,8] · Vladyslav Kavaka[6,7] · Lisa Ann Gerdes[6,7,8] · Klaus Dornmair[6,7,8] · Eduardo Beltrán[6,7,8] · Annette Oxenius[2] · Sai T. Reddy[1] · Doron Merkler[3,9] · Alexander Yermanos[1,2,3,11]

1 Department of Biosystems Science and Engineering, ETH Zurich, Basel, Switzerland

2 Institute of Microbiology, ETH Zurich, Zurich, Switzerland

3 Department of Pathology and Immunology, University of Geneva, Geneva, Switzerland

4 Institute for Biomedical Engineering, University and ETH Zurich, Zurich, Switzerland

5 Institute of Clinical Molecular Biology, Kiel University and University Medical Center Schleswig-Holstein, Kiel, Germany

6 Institute of Clinical Neuroimmunology, Faculty of Medicine, University Hospital and Biomedical Center (BMC), LMU Munich, Munich, Germany

7 Biomedical Center (BMC), Faculty of Medicine, LMU Munich, Martinsried, Germany

8 Munich Cluster of Systems Neurology (SyNergy), Munich, Germany

9 Division of Clinical Pathology, Geneva University Hospital, Geneva, Switzerland

10 Department of Neurology, University Hospital Ulm, Ulm, Germany

11 Center for Translational Immunology, University Medical Center Utrecht, Utrecht, Netherlands